

pubs.acs.org/JACS Article

Information-Rich, Dual-Function ¹³C/²H-Isotopic Crosstalk NMR Assay for Human Serine Racemase (hSR) Provides a PLP-Enzyme "Partitioning Fingerprint" and Reveals Disparate Chemotypes for hSR Inhibition

Stephany M. Ramos de Dios, Jared L. Hass, Danielle L. Graham, Nivesh Kumar, Aina E. Antony, Martha D. Morton, and David B. Berkowitz*



Cite This: J. Am. Chem. Soc. 2023, 145, 3158-3174



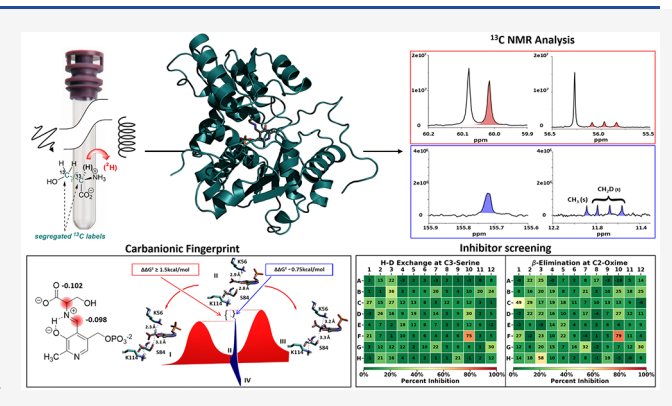
ACCESS I

III Metrics & More

Article Recommendations

s Supporting Information

ABSTRACT: The first dual-function assay for human serine racemase (hSR), the only bona fide racemase in human biology, is reported. The hSR racemization function is essential for neuronal signaling, as the product, D-serine (D-Ser), is a potent N-methyl D-aspartate (NMDA) coagonist, important for learning and memory, with dysfunctional D-Ser-signaling being observed in some neuronal disorders. The second hSR function is β -elimination and gives pyruvate; this activity is elevated in colorectal cancer. This new NMR-based assay allows one to monitor both α -proton-exchange chemistry and β -elimination using only the native L-Ser substrate and hSR and is the most sensitive such assay. The assay judiciously employs segregated dual 13 C-labeling and 13 C/ 2 H crosstalk, exploiting both the splitting and shielding effects of



deuterium. The assay is deployed to screen a 1020-compound library and identifies an indolo-chroman-2,4-dione inhibitor family that displays allosteric site binding behavior (noncompetitive inhibition vs L-Ser substrate; competitive inhibition vs adenosine 5'-triphosphate (ATP)). This assay also reveals important mechanistic information for hSR; namely, that H/D exchange is ~13-fold faster than racemization, implying that K56 protonates the carbanionic intermediate on the *si*-face much faster than does S84 on the *re*-face. Moreover, the 13 C NMR peak pattern seen is suggestive of internal return, pointing to K56 as the likely enamine-protonating residue for β -elimination. The 13 C/ 2 H-isotopic crosstalk assay has also been applied to the enzyme tryptophan synthase and reveals a dramatically different partition ratio in this active site (β -replacement: *si*-face protonation \sim 6:1 vs β -elimination: *si*-face protonation \sim 1:3.6 for hSR), highlighting the value of this approach for fingerprinting the pyridoxal phosphate (PLP) enzyme mechanism.

INTRODUCTION

Pyridoxal phosphate (PLP)-dependent enzymes constitute a critical component of the human proteome being responsible for some 4% of all EC-catalogued catalytic activities² and are the targets for important therapeutics from ornithine decarboxylase (difluoromethylornithine (DFMO); African sleeping sickness)³ to 3,4-dihydroxyphenylalanine (DOPA) decarboxylase (carbidopa; Parkinsonism)⁴ to 4-aminobutanoate (GABA) transaminase (vigabatrin, epilepsy, and drug addiction) to ornithine aminotransferase (hepatic carcinoma), and continue to emerge as potential new targets in bacterial, parasitic, and mammalian systems. All this said, PLP-dependent, human serine racemase (hSR) is the first bona fide amino acid racemase to be identified in human biology¹⁰ and is the source of D-serine (D-Ser), a potent coagonist of the N-methyl D-aspartate receptor (NMDAR) and a critical component of both normal and dysfunctional neuronal signaling. 11 The hSR protein converts L-Ser to D-Ser, and although L-glutamate is the primary agonist for the NMDAR, it has now been established that D-Ser is the most potent NMDAR coagonist, binding to the receptor at the "glycine site" approximately 2 orders of magnitude more potently than glycine itself. Both structural studies of the Gly-NMDAR and D-Ser NMDAR complexes¹² and "patch-clamp"-type experiments¹³ support this conclusion, underscoring the importance of careful regulation of the D-Ser concentration.

Proper homeostatic control of D-Ser levels is essential for long-term potentiation (LTP)¹⁴ associated with learning and memory.¹⁵ Conversely, a myriad of neurobiological disorders

Received: November 30, 2022 Published: January 25, 2023





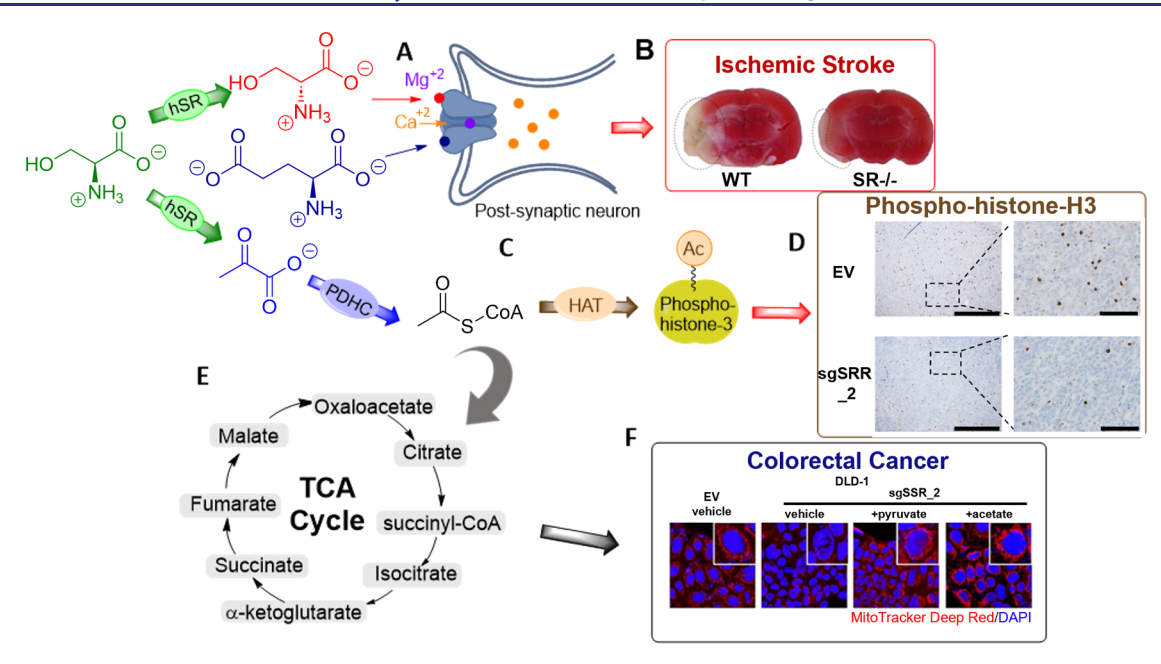


Figure 1. Biological relevance of hSR. (A) D-Ser serves as a coagonist of the NMDAR. (B) SR (-/-) mice exhibit reduced neuronal infarction in an MCAO-model for ischemic stroke (adapted with permission from ref 17, copyright 2010 Society for Neuroscience). (C) hSR-derived pyruvate leads to increased acetyl-CoA and resultant phosphohistone H3 acetylation. (D) Tumor lesions show higher levels of SRR EV and acetylated histone H3 than in sgSRR. (E) Higher acetyl-CoA levels also result from increased metabolism via the Krebs cycle. (F) MitoTracker Deep Red stains the mitochondrial mass of EV and SRR-KO. DLD-1 cells show less mitochondrial mass than is seen in SRR-KO. This is restored after incubation with pyruvate or acetate (figures in panels (D) and (F) are adapted with permission from ref 28, copyright 2020 Springer Nature).

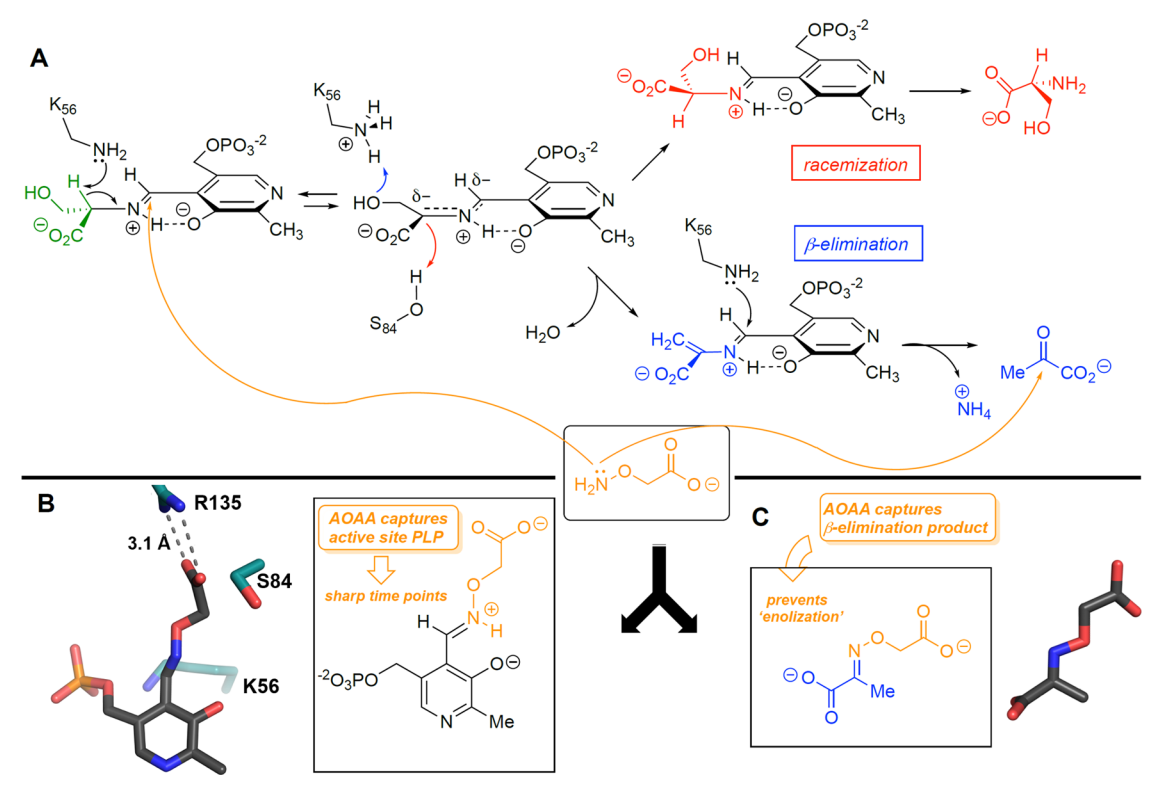


Figure 2. hSR mechanism and bifurcated aminooxyacetic acid (AOAA) quench. (A) Schematic view of the hSR mechanism; following transaldimination, α -deprotonation leads to a presumed carbanionic intermediate that bifurcates into β -elimination and racemization pathways. AOAA is added with the dual purpose of quenching the hSR reaction (B) and derivatizing the β -elimination product (C). Note that the AOAA molecule is ideally tailored for the hSR active site, as the AOAA-carboxylate presumably interacts with R135 while its hydroxylamine moiety engages the aldimine carbon of the PLP cofactor in a stable oxime linkage in the resting state of the enzyme as well as in aldimine intermediates along the reaction coordinate as illustrated here.

have been associated with hSR dysfunction. For example, hSR hypofunction correlates with schizophrenia and with a reduced expression of the cyclic adenosine monophosphate (cAMP)response-element-binding protein (CREB) (Figure 1A). 16 On the other hand, high levels of hSR and D-Ser may be excitotoxic and may lead to neuronal infarction in ischemic stroke. Consistent with this hypothesis, provocative model work from Dore, Snyder, Coyle, and co-workers showed a reduced infarct volume of SR-knock-out mice in a middle cerebral arterial occlusion model for ischemic stroke (Figure 1B).¹⁷ More recently, the Coyle lab provided compelling evidence that neurotoxic astrocytes associated with Alzheimer's disease overexpress SR, ^{18'} consistent with earlier observations of Mori¹⁹ and Panizzutti. ²⁰ These findings align with emerging reports of the role of hSR in neuronal disorders including amyotrophic lateral sclerosis (ALS),²¹ neuropathic pain,²² chronic social defeat stress,²³ post-traumatic stress (PTSD) syndrome,²⁴ and traumatic brain injury.²⁵ As hSR is the sole source of D-Ser in human neurobiology, there is clearly a need for better tools to study this enzyme and for inhibitors/ activators to modulate its activity as tools for chemical biology.

Interestingly, hSR catalyzes the β -elimination of L-Ser to pyruvate even more effectively than it racemizes L-Ser to D-Ser $(k_{\rm cat}/K_{\rm m}(\beta\text{-elim}):k_{\rm cat}/K_{\rm m}({\rm rac})\sim 4:1).^{10a,26}$ While the related β -elimination function of D-Ser to pyruvate has been implicated in regulating D-Ser levels,²⁷ noteworthy recent work from Morii and co-workers indicates oncogene-like behavior of hSR in colorectal cancer. These workers have shown that elevated acetyl-SCoA emanating from hSR-derived pyruvate both fuels elevated metabolism through the tricarboxylic acid (TCA) cycle and leads to histone H3 acetylation at lysine 27, preventing apoptosis (Figure 1C-F).24 Indeed, transcription regulation associated with the acetylation state at the H3K27 locus has been linked to colorectal cancer.²⁹ Perhaps related to these observations, a recent report identifies serine racemase as a possible oncogene in endometrial cancer.³⁰

We report here the first direct dual-function assay providing kinetic information that relates to both biologically relevant hSR functions and the deployment of this new NMR-based assay to screen for inhibitors of hSR. These studies provide an important fundamental tool development step in the quest for effective modulators of this important enzyme. There is currently great interest in finding inhibitors of hSR as tools for chemical biology³¹ to probe the roles of hSR in D-Ser regulation/homeostasis and to understand how hSR dysfunction contributes to the etiology of neurodegenerative disease and neoplasia. The quest for function-based inhibitors of PLP-enzymes^{26,32} also aligns well with a long-standing program in this research group that includes their effective deployment as chemical biological tools.^{9a}

Mechanistically, hSR follows the prototypical PLP enzyme trajectory (see Figure 2A for a schematic representation) with the resting state of the enzyme being an internal aldimine whereby the active site lysine, K56, holds the PLP cofactor in an internal aldimine linkage. The substrate, L-serine, displaces K56 in a transaldimination reaction to give the external aldimine. As is depicted in Figure 2A, K56 α -deprotonates this species leading to a presumptive carbanionic intermediate. Protonation on the *re*-face by S84 leads to D-Ser. We proposed that the p $K_{\rm a}$ of the serine-84 residue is lowered through a H-bond network to K114, 26 based upon an analogy with the Ser*cis*-Ser-Lys triad seen in structures of the signature amidase

enzyme family (see animation in the Supporting Information (SI)). On the other hand, protonation of the β -hydroxy group and β -elimination gives a bound enamine that after protonation, transaldimination, and imine hydrolysis yields a molecule of pyruvate and a molecule of ammonia. In this way, the dual functions of the hSR enzyme pass through a common putative carbanionic intermediate.

That said, to our knowledge, there has not yet been reported a dual-function assay for SR. Moreover, a survey of the literature indicates that all SR activity assays reported heretofore involve either the installation of a chromophore in the enzymatic product or the coupling of SR activity to that of one or two additional reporting enzymes. The most widely employed assays for SR monitor the β -elimination of either L-serine or, more commonly, of the faster unnatural substrate, L-serine-O-sulfate (L-SOS). In these assays, the pyruvate product is detected by reduction to L-lactate by lactate dehydrogenase (LDH) with the concomitant decrease in the absorbance at 340 nm as NADH is converted to NAD⁺. 10e,26,27,33 These assays measure exclusively β -elimination activity and take advantage of the nicotinamide cofactor chromophore associated with the LDH reporting enzyme.

Similarly, one racemization assay utilizes a doubly coupled assay that combines D-amino amino oxidase (DAAO) and peroxidase as sequential reporting enzymes, exploiting a dye cofactor, often Amplex Red, 26 associated with the peroxidase enzyme to produce a colorimetric or fluorometric output. Alternatively, several methods to detect the racemization function involve the covalent adduction of both L-Ser and D-Ser to give chromophoric species that can be detected spectroscopically. These include condensation with the chiral Marfey reagent, 10e the adducts of which are separated on reverse phase-high-performance liquid chromatography (RP-HPLC) or adduction with o-phthaldialdehyde (OPA)/ β mercaptoethanol³⁴ or fluorescein isothiocyanate (FITC), followed by capillary electrophoresis using a γ -cyclodextrinbased chiral matrix, and detection by UV/absorbance or laserinduced fluorescence, respectively.

RESULTS AND DISCUSSION

As noted, these SR assays are all single-function assays; we disclose here the first dual-function SR assay of which we are aware. As will be delineated, the assay relies on the strategic use of $^{13}\text{C-labeling}$ at both C2 and C3 of L-Ser so that no coupling enzyme or chromophore is needed. This assay is performed in a 200 μL volume across a 96-well format that then, via liquid handler technology, translates into a 96 \times 3 mm² array of NMR tubes in an autosampler rack. In this manner, we can assay a significant number of conditions in parallel. To ensure this level of throughput, we found it valuable to use a fixed time point per tube. We present our information-rich NMR-based assay that can independently read two important activities of hSR simultaneously.

Bifurcating Quench with Aminooxyacetic Acid (AOAA). As is illustrated in Figure 2, the new hSR assay utilizes AOAA to produce crisp time points and provide tight signature NMR peaks for the β -elimination product, as well as sharp internal standards to ensure a clean quantitation of this enzymatic function and a favorable signal/noise (S/N) ratio. Specifically, AOAA is a well-tuned irreversible inactivator of the hSR enzyme as it bears a carboxylate functional group (FG) that is expected to engage the R135 residue in the active site in a salt bridge and, in this way, deliver the hydroxylamine

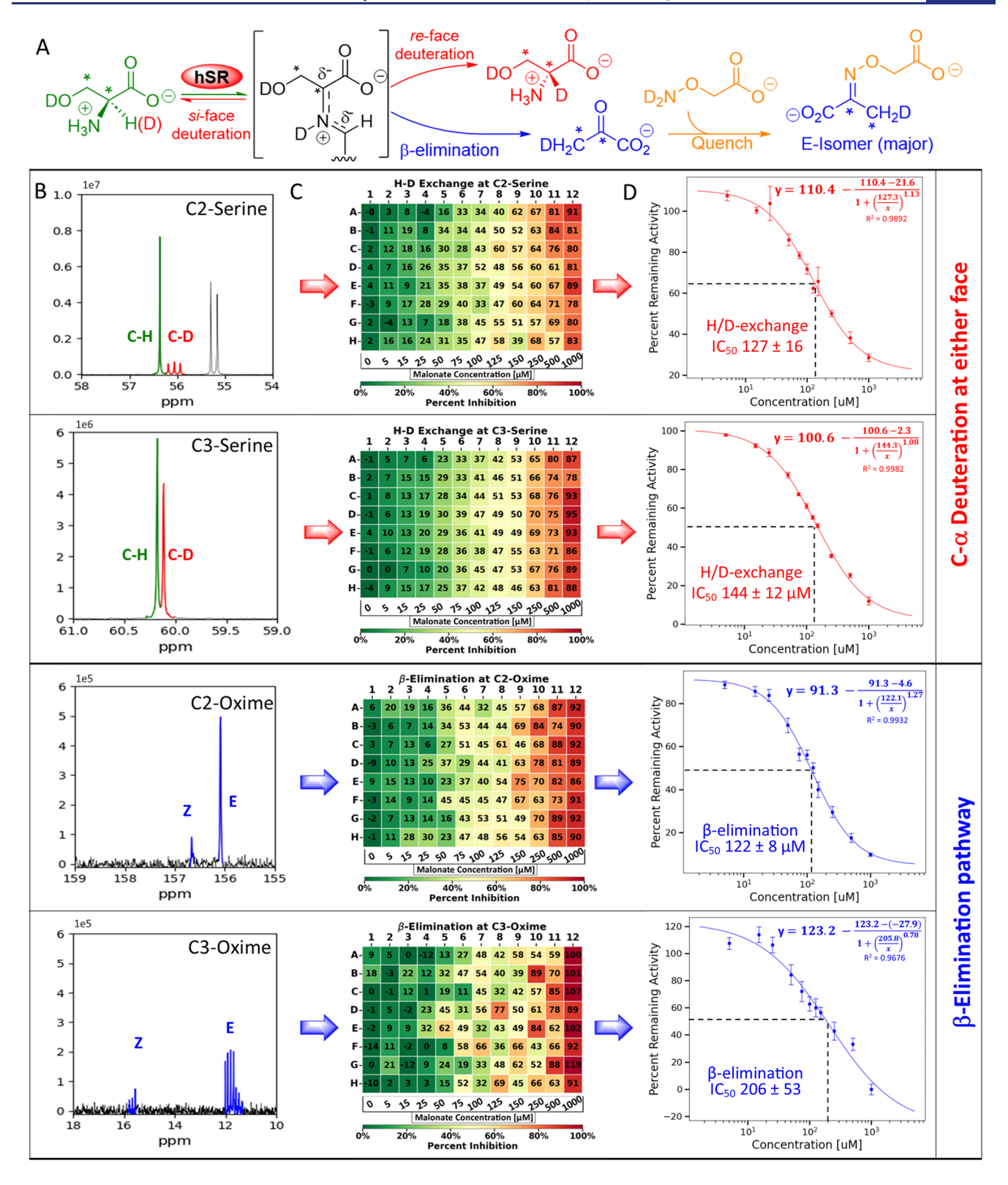


Figure 3. β -Testing the segregated ¹³C-dual label assay for hSR. (A) Isotopically enriched serine has three possible fates upon reaching the carbanionic intermediate, *si*-face protonation (simple H/D exchange), *re*-face protonation (racemization), or β -elimination to pyruvate, which is subsequently captured as the oxime. (B) Segregated dual ¹³C-labeling at C2 and C3 gives four readouts, two for each function. (C) Signal using the known inhibitor, malonate, at various concentrations. The assay is run in standard, disposable 96-well microtiter plates (200 μL assay volume; 220 μL after quenching). The heat maps shown are designed to represent this 96-well plate format, and the numbers depict the percent inhibition for the compound in the given well. (D) C3-position was selected for the H/D exchange readout and the C2-position was selected for the β -elimination readout as they provide the most tightly reproducible datasets with the narrowest experimental uncertainty envelopes.

nitrogen to the C-4'-carbon of the cofactor, thereby facilitating rapid capture of the cofactor in an oxime linkage. The formation of this active site-directed salt bridge between the AOAA-carboxylate and R135 is supported by molecular docking (Figure 2B) and is consistent with the crystallographic record (Protein Data Bank (pdb) 3L6B) showing that malonate forms a similar salt bridge when bound to mammalian SR. Moreover, an AOAA-PLP oxime is seen in the active site of inactivated GABA transaminase with a similar salt bridge to R141 there (pdb 1SFF). This proposal is also consistent with previous molecular modeling results from our group on hSR suggesting that the β -carboxylate of the excellent substrate L-threo- β -hydroxyaspartate (L-THA) engages in such a salt bridge with R135, positioning the L-THA both for transaldimination and subsequent β -elimination.

The AOAA not only captures the hSR-PLP by attacking and "transaldiminating" at C-4', but it also captures the β elimination product pyruvate as an AOAA-pyruvate oxime that can be quantitated easily (Figure 2C). Two diagnostic ¹³C-signals at C2 (C=NOR) and C3(Me) of this pyruvatederived oxime appear in open regions of the NMR spectrum [~156-157 and 12-16 ppm, respectively; two geometric oxime isomers are observed with the E-(trans)-isomer predominating as determined by nuclear Overhauser enhancement spectroscopy (NOESY)—Figure S11]. The AOAAoxime offers additional advantages as it essentially chemically freezes out deuterium exchange at the α -carbon (see Figure S8) and the attendant splitting that this gives (see Figure S9 for a representation). In fact, control experiments (Figure S10) show that pyruvate itself readily undergoes nonenzymatic α deuteration, particularly at higher pH values (7.5-8.5) leading ultimately to broadening of the C3-signal and reduced S/N. To further optimize S/N and reduce potentially artefactual hydrogen-coupled signal enhancement, the T_1 delay was optimized (8 s) and an inverse-gated pulse program was used. The addition of excess AOAA at the quench lowers the pH from the assay pH of 8 to 2-4, which both slows down pyruvate deuteration (one D should be introduced in the hSRmediated β -elimination process in the enamine protonation step) and favors its capture as the stable oxime. Moreover, control experiments (Figure S6) reveal that the lower pH sends the two triethanolamine (TEA) carbon peaks upfield and sharpens them, allowing these peaks to serve as internal standards.

Dual ¹³C-Labeling, ¹³C/²H-Crosstalk hSR NMR Assay. The assay utilizes ¹³C and ²H-labels strategically in several important ways that provide for the high S/N and specificity of information: (1) Specifically, ¹³C-enrichment spotlights the enzymatic reaction chemistry alone, against a carbon-rich background, both in this in vitro system and potentially in more complex systems as well. (2) Site-specific labeling pinpoints functional group (FG)-critical loci in the educt/ product that are diagnostic for the specific chemistry being probed. For example, for the β -elimination reaction of hSR, in terms of the ¹³C2 and ¹³C3-labels installed, the chemistry proceeds via FG transformations at C2 from CH(NH₂)-(CH₂OH) to C=O to C=NHOR and at C3 from CH₂OD to $(C=O)CH_2D$ to $(C=NHOR)CH_2D$ (Figure 3B); the former signal migrates well downfield and the latter well upfield, in parallel with the chemical transformation. (3) ¹³C-label isolation, i.e., using an equimolar ratio of ¹³C2 and ¹³C3-single labels across the substrate population, ensures that both positions are amplified 50-fold above the background ¹³C noise

and abrogates $^{13}\text{C}-^{13}\text{C}$ splitting across C2 and C3, ensuring sharp signals. Finally, both (4) $^{13}\text{C}/^2\text{H}$ -splitting, leading to the characteristic 1:1:1 triplet for C2 associated with C α -deuteration, and (5) the $^{13}\text{C}/^2\text{H}$ -shielding effect, leading to upfield chemical shifts at both $^{13}\text{C2}$ (attached carbon) and $^{13}\text{C3}$ (adjacent carbon) are direct reflections of the $^{13}\text{C}-^2\text{H}$ crosstalk that is at the core of the assay.

 β -Test of the ¹³C/²H-Crosstalk-Based hSR Assay. This is an information-rich assay; the dual labeling system at C2 and C3 enables two independent readouts for each function as can be seen from the spectral data in Figure 3. For the Cα-proton exchange, one sees upfield-shifted signals for ¹³C2 (56 ppm) and ¹³C3 (60 ppm); for β -elimination, one sees the characteristic AOAA-oxime peaks in open spectral windows for ¹³C3 (12 ppm, ¹³CH₂D) and ¹³C2 (156 ppm, ¹³C=NOR) (Figure 3B). To ensure that the new assay is well-behaved, we have taken time points (AOAA quench) every 5 min across the early conversion (ν_0) domain, and we observe linearity (see Figure S13 and the surrounding discussion for details).

We next set out to β -test the assay as an inhibitor screen, utilizing the best-known hSR inhibitor, malonate, across a range of 12 concentrations from 0 to 1000 μ M in 8 replicates in the 96-well plate format (Figure 3C). Each well was read in four different ways based on the four diagnostic signals described. The relative integrals of these characteristic peaks from the primary NMR spectra were translated into a 96-well plate heat map format using a Python program in a Pandas DataFrame. All four independent signals display a color gradient across the heat map typical of such an inhibitor titration and report out an IC₅₀ for malonate in the 100–200 μ M range consistent with literature values (Figure 3C)^{33a,3733a,37} highlighting the value of the dual label format.

For the C α -exchange function, the ¹³C3-signal was found to yield data with a smaller uncertainty envelope, particularly with the Lorentzian curve fitting to ensure baseline resolution. The C3-deuterated serine peak gives a sharper peak than the C2triplet and highlights the value of reading a deuteration event at the carbon adjacent to the locus of C-D bond formation, a subtle but important point. At this adjacent carbon, the shielding effect of the introduced deuterium is felt and seen at the resolution of a 700 MHz (175 MHz for ¹³C) instrument, without the signal broadening associated with C-D splitting that is seen at the attached carbon. Only the ¹³C3-oxime signal shows really significant uncertainty (gives $IC_{50} = 206 \pm 53$ μ M) of the four independent readouts, owing to the most significant broadening due to pyruvate deuteration beyond the initial monodeuteration in the hSR-catalyzed reaction, as has been discussed. Interestingly, the ¹³C2-"quaternary" carbon signal from the oxime was the most reproducible signal for the β -elimination function, providing a clear sharp peak that integrates well (Figure 3D).

On the Putative Carbanionic Intermediate in hSR. By the classical Dunathan hypothesis, alignment of the $C\alpha-H$ bond with the extended π -system of the cofactor in the external aldimine complex should weaken this bond in the hSR active site and allow for *si*-face deprotonation by the K56 active site base. This ordinarily gives a fully delocalized "quinonoid" intermediate in active sites for which an Asp or Glu residue protonates the PLP-pyridine nitrogen as is commonly seen in fold-type I PLP enzymes. However, hSR is in the fold-type II family of PLP enzymes in which a Ser-residue is typically juxtaposed with the PLP-ring nitrogen, likely forming only a weak H-bond, ³⁸ disfavoring full delocalization of the electron

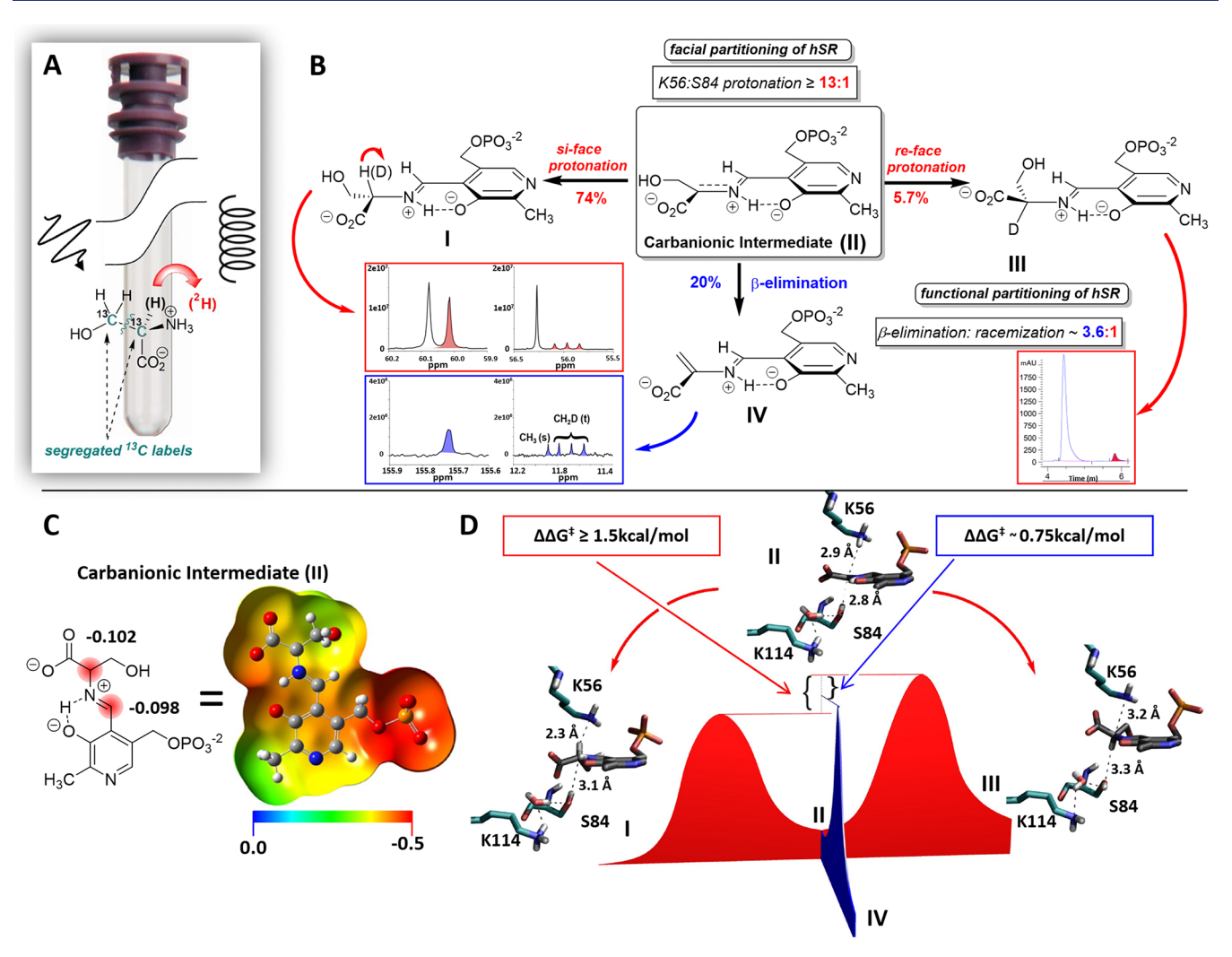


Figure 4. Dual label 13 C- 2 H crosstalk-based hSR assay provides mechanistic insight. (A) Schematic illustration of the segregated dual (13 C- 13 C3)-labeled, deuterium exchange principle underlying critical aspects of the assay. (B) Observed tripartite partitioning of the carbanionic intermediate: *si*-face-protonation vs *re*-face protonation vs β-elimination. The assay reveals the most sensitive measure of hSR activity with its native substrate yet seen (predominantly *si*-face-protonation). A comparison with racemization alone (Marfey assay-SI) is consistent with a facial partitioning ratio of (K56) *si*-face-protonation: (S84) *re*-face-protonation of ~12.8:1. This gives an overall experimental tripartite partition ratio of 12.8:3.6:1. (C) Putative carbanionic intermediate charge distribution (Gaussian). (D) Schematic free energy diagram for the tripartite partitioning observed showing the L-Ser external aldimine (I), putative carbanionic intermediate (II), p-Ser external aldimine (III), and β-elimination pathway (IV). That *si*-face protonation of the carbanionic intermediate is favored by 12.8:1 over *re*-face protonation corresponds to $\Delta \Delta G^{\ddagger} = 1.50$ kcal/mol at room temperature (RT), favoring reprotonation on the *si*-face, an activity not previously observed for hSR. This model assumes that relative rates seen reflect proton transfer chemistry.

density in the carbanionic intermediate. Toney and co-workers pointed out early on that there might well be PLP enzymes that generate carbanionic intermediates that are not fully delocalized.³⁹ As pertains to the studies reported herein, this work suggests that fold-type II PLP enzymes that perform β elimination or replacement chemistry on L-Ser, such as the title enzyme, hSR and tryptophan synthase (TS), cystathionine β synthase (CBS), tyrosine phenol lyase, or tryptophanase might proceed via a less delocalized, carbanionic intermediate. Consistent with this thinking, such a more localized carbanionic intermediate has been observed for CBS by Banerjee, Smith, and co-workers crystallographically at higher pH^{9b} and for TS in elegant solid-state NMR crystallography experiments by Mueller, Caulkins, and co-workers. 40 On the basis of these observations and the similarities of these enzymes to hSR (see Figure S16 and the surrounding discussion of these carbanionic intermediates), one might

expect that such a localized carbanionic intermediate obtains in the hSR active site. The data provided here are consistent with the reversible formation of such an intermediate (Figure 4) in the hSR active site.

Tripartite Partitioning of the Putative Carbanionic Intermediate-Mechanistic Insight from the Rapid H/D-Exchange Seen. During preliminary experimental runs with the 13 C/ 2 H NMR assay for hSR, it became evident that the rate of α-deuteration observed far exceeded what one would expect based upon the typical 4:1 ratio for β-elimination to racemization observed by us and others for this enzyme. 26,27 The observed ratio by NMR appeared to be almost 4:1 in the opposite direction strongly suggesting that we might be observing a previously unseen α-proton-exchange reaction leading to α-deuterated L-Ser, a reaction that would have gone undetected with all previously reported assays for this important enzyme.

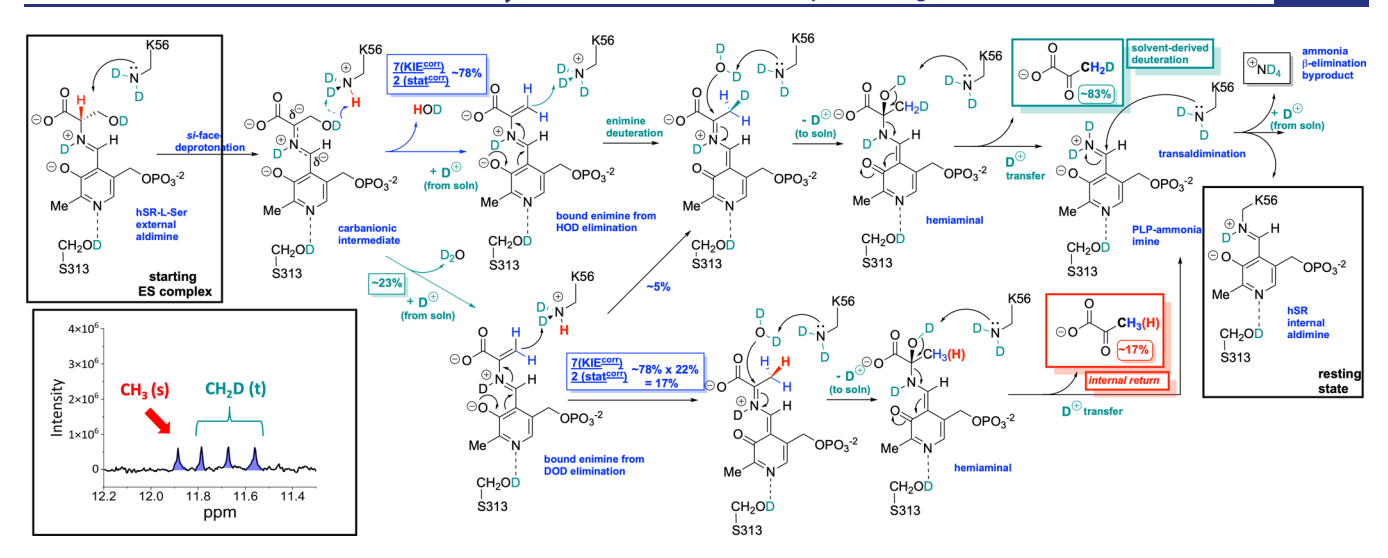


Figure 5. Dual label 13 C-D crosstalk-based hSR assay provides mechanistic insight for the β -elimination reaction. The 13 C-signatures seen in the NMR assay for the 13 C3 methyl of the AOAA-oxime of the pyruvate β -elimination product (lower left-hand corner; major geometric isomer) include an upfield triplet (1:1:1; 11.7 ppm) and a downfield singlet (11.9 ppm), consistent with the formation of $\sim 80\% - O_2C(C=O)CH_2D$ (t) and $\sim 20\% - O_2C(C=O)CH_3$ (s), featuring the characteristic shift perturbation and multiplicity associated with α -deuteration. The mechanism for β -elimination shown is aligned with these observations and utilizes K56 for (i) *si*-face deprotonation; (ii) β -OH leaving group protonation; and (iii) enamine protonation, consistent with the "minimum base number rule" of Hanson and Rose. Assuming a complete exchange of K56 with the D₂O solvent and a primary kinetic isotope effect (KIE) of 3–7 for H+-transfer over D+-transfer from the $-ND_2H$ group, one arrives at a prediction of $\sim 20-25\%$ internal return of the α -proton of L-Ser to the C3-position of the pyruvate β -elimination product. [Note: for clarity, the α -proton of L-Ser is painted red in the scheme so that the internal return pathway ($\sim 20\%$) and its wash-out pathway ($\sim 80\%$) can be easily followed].

To probe this carefully, we next set out to compare the rate of H/D exchange being observed experimentally directly with the rate of L-Ser \rightarrow D-Ser racemization in the same sample. This experiment was run in triplicate under standard conditions [30 mM L-Ser (segregated ¹³C-labeling at C2 and C3; 50% enrichment each), 2.5 mM adenosine 5'-triphosphate (ATP), 5 mM MgCl₂, 150 mM KCl, 200 mM TEA buffer, pH 8, 10% dimethyl sulfoxide (DMSO)—400 μ L total volume]. After addition of hSR (\sim 27 mU—L-Ser β -elim. units), the enzymatic reaction was run for 30 min, then split into two equal portions; one portion was subjected to the usual AOAA quench and the other to a thermal quench (5 min, 70 °C water bath). The AOAA quenched portion was analyzed by ¹³C NMR at 175 MHz (700 MHz instrument), whereas the thermally quenched portion was filtered and then subjected to derivatization with the Marfey reagent/RP-HPLC, as described in detail in SI. Figure 5 depicts the results of these parallel ¹³C NMR/Marfey derivatization runs. Detailed analysis shows that $74 \pm 0.8\%$ of the deuterated serine is L-Ser, whereas only 5.7 \pm 0.6% is D-Ser, revealing that the putative carbanionic intermediate passages ~13-fold faster in the direction of L-Ser (simple H/D exchange) than in the direction of D-Ser (racemization). The remaining hSR chemistry consists of 20 \pm 3.4% β -elimination. These results provide the first measure of the tripartite partitioning of the putative carbanionic intermediate, yielding a ratio of 1:3.6:12.8 for racemization/ β -elimination/internal si-face reprotonation, assuming that chemistry emanating from the putative carbanionic intermediate is fully rate-limiting (Figure 4B,D).

Putting these results in context with the literature, it is worthy to note that Nitoker and Major had previously endeavored to theoretically probe the mechanism of hSR using a multiscale modeling approach.⁴¹ To obtain a free energy profile for the hSR reaction, a hybrid quantum mechanics/molecular mechanics (QM/MM) molecular dynamics simulation was run with umbrella sampling. The

authors arrive at a prediction that, indeed, si-face protonation (K56) of the hSR-derived carbanionic intermediate would be favored over re-face protonation (S84) by 1.9-2.9 kcal/mol for the CM and QM estimates, respectively. The current experimental data support and build upon this calculation, demonstrating for the first time that, indeed, for L-Ser, si-face deprotonation/reprotonation is in rapid equilibrium with respect to racemization for hSR. This is almost certainly a testament to the greater efficiency with which the active site K56 si-face base protonates the putative carbanionic intermediate in comparison to the S84 re-face base. Perhaps most importantly, the rapid si-face reprotonation chemistry seen here constitutes the most sensitive measure of active site chemistry for human serine racemase yet observed with the native substrate, L-serine. One might view the newly uncovered H/D exchange activity as a pseudoracemization half-reaction, and effectors that inhibit this activity will almost certainly inhibit racemization, as well, suggesting that this is an excellent activity window to probe in a screen, as is demonstrated herein.

Probing Internal Return in the *β*-Elimination Pathway for hSR. As noted at the outset, in addition to generating the important neuronal signaling molecule, D-serine, via its racemization function, hSR also generates pyruvate via its second, β -elimination function, and this activity is especially pronounced in colorectal cancer. In addition to the *si-/reface H/D* exchange activity discussed above, this segregated ¹³C-dual labeling assay also gives rise to two diagnostic signals for β -elimination in the ¹³C-2 C=NOR and the ¹³C3 methyl peaks (Figure 3).

When the assay was run diagnostically, under standard conditions as just described, $\sim 20\%$ β -elimination was seen, giving a 3.6:1 rate ratio for β -elimination to racemization, similar to what has been seen both in our own experience and in other laboratories using the steady-state kinetic analysis.

However, by providing for ¹³C/²H crosstalk, this assay provides a level of mechanistic information not attainable from previously available assays, also as regards this β elimination pathway. Specifically, as is shown schematically in Figure 5, for the β -elimination of L-Ser by hSR, the mechanism is expected to begin from L-Ser α -deprotonation at the si-face by K56-ND₂ to give the common carbanionic intermediate. Then, presumably the β -OH leaving group must be protonated, and parsimony would argue for the K56-ND₂H + group to fulfill this function by pivoting modestly across the si-face. The probability for H+ transfer over D+ transfer to the leaving water molecule is estimated to be ~78% (3.5:1), assuming a primary kinetic isotope effect $k_{\rm H}/k_{\rm D} \sim 7:1$ (classical harmonic oscillator approximation value for a rate-limiting primary H/D KIE) in favor of hydrogen and a statistical preference of 1:2 in favor of deuterium.

This leaves 22% of a K56-ND₂H+ species (lower pathway; loss of D₂O) and 78% of a K56-ND₃+ species (upper pathway, loss of HOD) available for the third and final role of the si-face base; namely, protonation of the extended enamine-like intermediate. From this 22% of the K56-ND₂H+ species that still retains the original $^{13}\text{C2-}\alpha\text{-proton}$ (H+, lower pathway), there is now a 78% probability of internally returning that proton to ¹³C3 of the pyruvate formed. This corresponds to an \sim 17% probability (0.22 × 0.78 = 0.17) of internal H-return (and an ~83% probability of D-introduction). Note that if one assumes a KIE of ~5:1 for protonation from the K56-ND₂H+ group, one obtains an estimate of 21% internal return, and if one assumes a KIE of $\sim 3:1$, then one would predict a 24% internal return. Note that in the ¹³C-²H crosstalk NMR experiment, we reproducibly see a pattern of $\sim 20-25\%$ ¹³CH₃ (downfield singlet) and 75-80% CH₂D (upfield 1:1:1 triplet) at the methyl group of the pyruvate-AOAA oxime (lower lefthand corner, Figure 5), consistent with the mechanism delineated in detail in Figure 5.

The mechanism just described for hSR-catalyzed β -elimination from L-Ser ascribes three roles to K56 along the si-face: (i) α -deprotonation, (ii) β -OH protonation, and (iii) extended enamine protonation to give the pyruvate methyl group. While additional experiments are surely warranted to test this proposed mechanism, this postulate is not only consistent with the $^{13}\text{C}/^2\text{H}$ crosstalk signatures seen here, but this mechanism would also appear to follow the "miminal base number rule" articulated by Hanson and Rose 42 in putting forward principles of maximum parsimony in the evolution of catalytic efficiency for enzyme catalysis.

This pattern has been noted by others in β -elimination reactions, for example, by Cane for the polyketide synthase β -dehydratase mechanism wherein a catalytic base (His) is postulated to perform both the α -deprotonation and β -LG protonation functions. This postulate is also consistent with a recent elegant ssNMR study by Mueller, Caulkins, and coworkers in which good evidence was provided for TS, the active site-Lys protonates, the β -LG of serine, as well. In terms of the facial selectivity of PLP-enzyme-dependent β -elimination reactions, both tyrosine phenol lyase and tryptophanase are known to catalyze β -elimination from L-Ser with protonation from the same face of the putative extended enamine intermediate from which the OH left, consistent with the single base mechanism presented here.

hSR Inhibitor Candidate Screening. Given the important biological activities of hSR, there has been great interest in developing inhibitors. ^{31,37b,46} There are only two

medium to high throughput assays for hSR binding yet reported, to our knowledge. Toney, Kurth, and co-workers used a one bead-one compound approach to screen >10,000 bead-bound peptides, identifying pseudotripeptidic inhibitors. 37a And recently, Bax and co-workers used an X-ray crystallographic soaking screen of 600 XChem fragments at 150 mM in 30% DMSO to identify a half-dozen fragments that bind in an array of pockets, including two that bind at the dimer interface with mM IC₅₀ values.^{31a} Two fragments, x0482 and x0458, display IC₅₀ values of 5.1 \pm 0.8 and 10.6 \pm 1.4 μ M and bind at a pocket flanking the ATP-binding pocket and the dimer interface (see Table S3 for a full accounting of the Bax results). From the wide range of activity-based screening efforts in the literature, the most potent inhibitors yet identified include malonate $(K_i \sim 20-120 \ \mu\text{M})^{33a}_i$ dichloromalonate $(K_i \sim 20 \ \mu\text{M})^{47}$ and L-erythro- β -hydroxyaspartate (L-EHA; $K_i \sim 30 \ \mu M$).

There is clearly a need for new types of lead compounds for hSR inhibition. To this end, we report here on the application of the new ¹³C-²H-isotopic crosstalk to the screening of a structurally diverse library of 1020 inhibitor candidates with the aim of exploring the efficacy and dynamic range of the assay and identifying new inhibitors for this enzyme. Library design was motivated by a desire to achieve structural diversity⁴⁸ with an eye toward natural productlike scaffolds,⁴⁹ including heterocycles such as quinazoline, indole, benzopyran,⁵⁰ chromane,⁵¹ benzimidazole, and pyrimidine. An additional consideration was given to systems that might be assembled in a modular fashion by diversity-oriented synthesis (DOS)⁵² (see the SI for the complete library profile).

Several Disparate Chemotypes for hSR Inhibition Emerge. In the event, the 1020-compound library screen led to several distinct chemotypes for further exploration, as will be discussed sequentially here. We spiked plate I intentionally with a couple of potential malonate analogues; namely, phosphonoacetate 1 (I-C05) and diethyl phosphonate acetate 2 (I-E08), each run at a high concentration (100 mM), into their respective wells. IC₅₀ plots for both H/D exchange and β elimination 1 and 2 conveniently served as positive controls. This gave us the opportunity to establish our protocol for generating the heat map readouts (Figure S18B) and to exploit the assay to simultaneously generate IC₅₀ plots. (Note: all IC₅₀ graphs are plotted in the semilog format after fitting the data to a four-component Hill-type dose-response curve. 53) These compounds displayed only weak affinity for hSR with phosphonacetate 1 giving $IC_{50}(H/D\text{-exchange}) = 89 \pm 35$ μ M and IC₅₀(β -elimination) = 39 \pm 2 mM (Figure S18A). Diethyl phosphonoacetate 2 showed slightly better numbers, coming in at $IC_{50}(H/D\text{-exchange}) = 95 \pm 10$ and $IC_{50}(\beta$ elimination) = 96 ± 19 mM (Figure S18C).

Biginelli Adduct. During the preliminary screening, 3 (II-C03) otherwise denoted here as a Biginelli adduct⁵⁴ showed significant precipitation at the 1 mM concentration (10% (v/v) DMSO) generally used for screening (see Figure S19A). To address this problem, compound 3 was re-examined at a saturating concentration of 30% (v/v) DMSO. This allowed for increased solubility and at these saturating conditions (~8.4 mM) showed ~50% inhibition. Because of solubility limitations, the inhibition data for 3 were plotted in the bar graph form (Figure S19B) and are consistent with an IC₅₀ between 5 and 10 mM for both reactions; H/D-exchange (red bars) and β-elimination (blue bars).

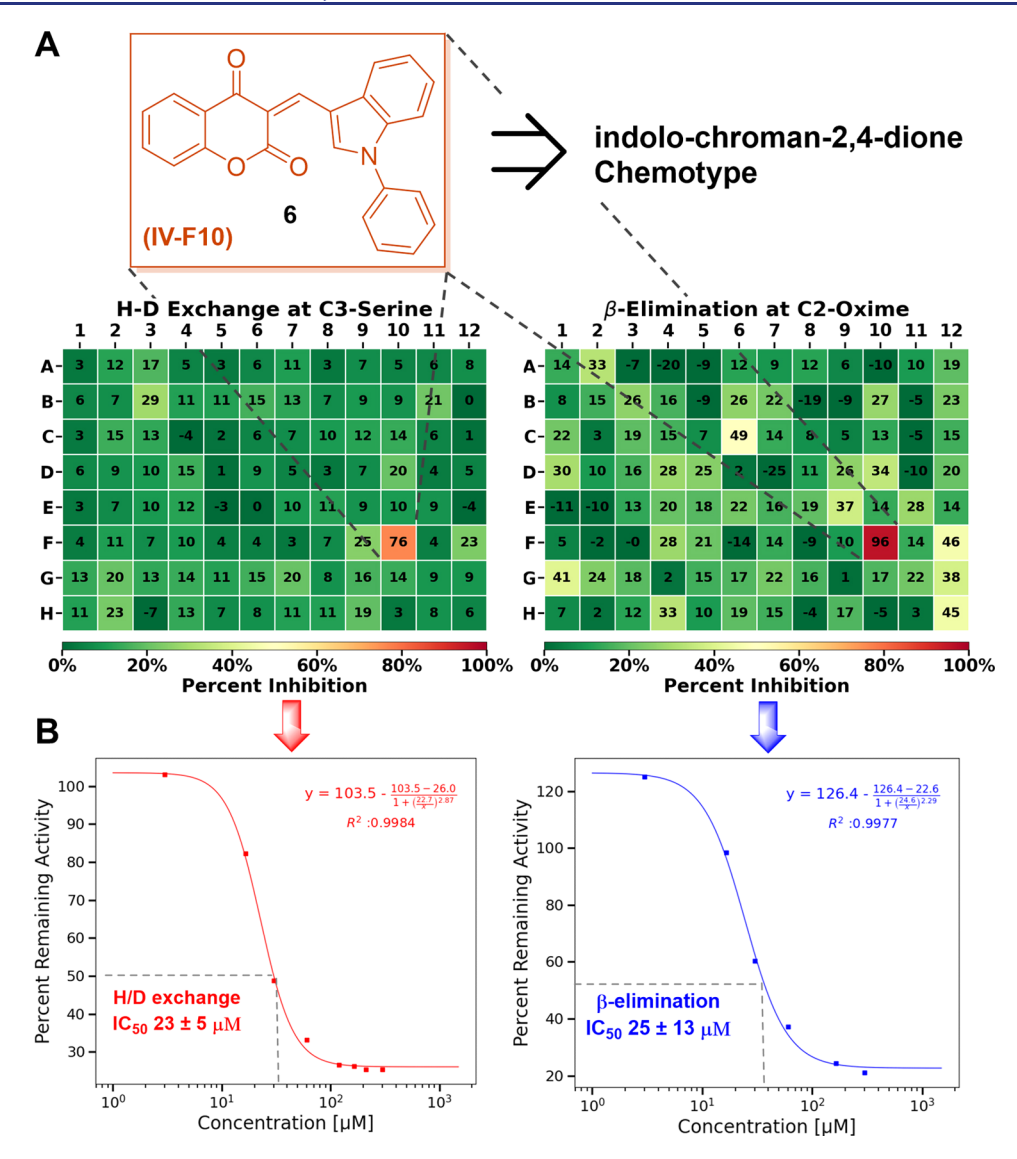


Figure 6. Library screening with the 13 C $^{-2}$ H crosstalk hSR assay-*N*-phenyl indolo-chroman-2,4-dione (6). (A) Heat map for a plate in a 96-well plate format for H/D exchange and the β-elimination reaction showing compound **IV-F10** with 76–96% inhibition at 1 mM. (B) IC₅₀ analysis for entry **IV-F10** (6).

5-(Aryl)Furfuryl Aminotetrazole Chemotype. As was noted earlier, a number of carboxylate surrogates were included in the library, and among these, a series of 5-(aryl)furfuryl aminotetrazoles, varying only in the substitution in the arene ring, were distributed across plate III and quite a few showed evidence of inhibiting hSR in the screen (Figure S20B,D). The most prominent among these was III-F05 (4) showing ~70% (several runs, see \$20D) inhibition@1 mM for the H/D exchange and β -elimination reactions (Figure S20B). Interestingly, entry III-G12 (5) featuring a very similar structure but differing only in the positioning of the two aromatic chlorine substituents (3',5'- vs 2',4'-) showed almost no inhibition in the screen at 1 mM. Interestingly, as is reflected in the bar graph in Figure S20D, across the range of 5-(aryl)furfuryl aminotetrazole family members on plate III, there is quite a structure-activity relationship (SAR) seen in this family. Holding the furfuryl and aminotetrazole moieties fixed (painted red and green in Figure 8) and varying only the substituents' phenyl ring (painted blue), one sees inhibition ranging from 10 to 67% inhibition at the 1 mM screening

concentration, depending on the precise constellation of substituents.

Indolo-chroman-2,4-dione Chemotype. The most interesting "hit" in the library turned out to be *N*-phenyl indolo-chroman-2,4-dione 6 (IV-F10) showing ~76% inhibition for the H/D-exchange reaction and nearly complete inhibition for the β -elimination reaction at 1 mM (Figure 6A). A complete titration using the new 13 C/ 2 H-isotopic crosstalk assay gave IC $_{50}$ (H/D-exchange) = 23 ± 5 μ M for H/D exchange and IC $_{50}$ (β -elimination) = 25 ± 13 μ M (Figure 6B). This result was quite promising as this is comparable to the most potent hSR inhibitors yet described (see the tabular collection in the SI), as has been discussed. This observation spurred us on to build out some initial SAR around this structure, as will be described below. Figure 7 provides an overview of the best inhibitors found through this screen/hit elaboration approach, as is described in more detail below.

"Hit Chemotype" Elaboration-Modular Syntheses. The three most interesting chemotypes identified in the 1020-compound screen represent readily diversifiable scaffolds

4 (III-F05)
$$K_{I} = 380 \pm 13 \, \mu M$$
Non-competitive

Non-competitive

Non-competitive

Non-competitive

Non-competitive

Non-competitive

Non-competitive

Non-competitive

Non-competitive

Figure 7. hSR inhibition profile of the best chemotypes. Library screening and follow-on synthesis yielded the above results. Both the 5-(aryl)furfuryl aminotetrazole and indolo-chroman-2,4-dione chemotypes display noncompetitive inhibition (see the SI for a complete set of steady-state kinetic data).

as these are constructed through modular syntheses that allow for structural variation across two to three domains of the target by a judicious choice of synthetic building blocks. Compound 3, though only a modest binder, is the product of a Biginelli condensation, a "multicomponent" reaction in which thiourea, a β -keto ester, and an aryl aldehyde are condensed in a one-pot procedure, leading to the product via sequential

imine formation, Mannich condensation, and nucleophilic ring closure, as is illustrated schematically in Figure 8.

As noted above, by far the most interesting chemotype to emerge from this screen was the indolo-chroman-2,4-dione family. The N-phenyl member of this family (6) emerged as the most interesting "hit" in the 1020-compound library screen, and this compound could be synthesized de novo in larger quantities for kinetics studies through Cu-mediated Narylation to introduce the N-Ph group, followed by aldol condensation with 4-hydroxycoumarin and in situ thermal dehydration to give 6. This promising lead scaffold also proved to be amenable to SAR studies. Accordingly, the indole N-H in indole-3-carboxaldehyde was deprotonated and alkylated (BnBr, i-BuBr, MeI), followed by the aldol/dehydration chemistry with 4-hydroxycoumarin, as before, to smoothly generate the N-benzyl (7), N-i-Bu (8), N-methyl (9), analogues of 6 (Figure 8—see the SI for full synthetic details and characterization).

Hit Verification by Independent Steady-State Kinetic Analysis. Two Families of Noncompetitive hSR Inhibitors *Emerge.* In assessing the results of the ¹³C-based NMR screen, including the information-rich, dual-function IC50 curves (Figures S18-S20 and 6), it became clear that we had identified a set of inhibitors with affinities for hSR across several orders of magnitude, with two classes, in particular, the 5-(aryl)furfuryl aminotetrazoles (4 and 5) and N-phenylindolo-chroman-2,4-dione (6) displaying both the requisite affinity and solubility to warrant further kinetic characterization. Of course, the newly synthesized N-alkyl indolochroman-2,4-diones 7-9 were also well suited to such detailed kinetic analysis. With appreciable synthetic quantities of all of these compounds in hand, as described, we examined compounds 4 and 5 (see Figure S21), as well as 6-9 (see Figure S22) by complete, steady-state enzyme kinetic analysis for the β -elimination of L-serine-O-sulfate (L-SOS), the most common substrate for measuring hSR activity (see the SI for details and Figure 7 for a summary of the kinetic constants and modes of inhibition observed).

The most exciting result from the NMR screen was *N*-phenyl indolo-chroman-2,4-dione (6), which again performed

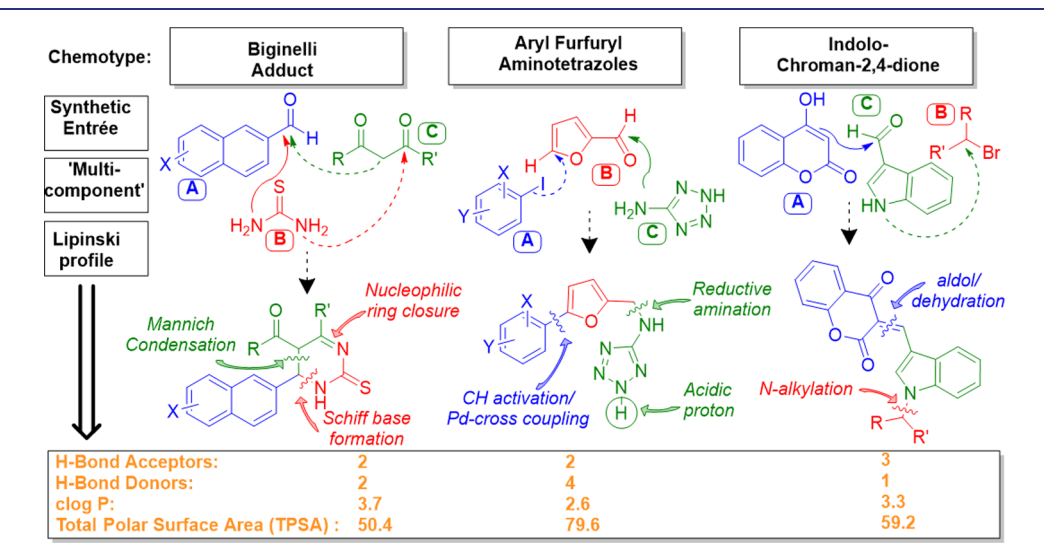


Figure 8. ¹³C/²H crosstalk NMR assay for hSR inhibition—DOS-ready "hit chemotypes". Illustration of the synthetic entry into the "hit" compounds by a multicomponent synthesis. The compounds display characteristics that are in alignment with Lipinski's rule of 5. (Detailed synthetic information can be found in the SI).

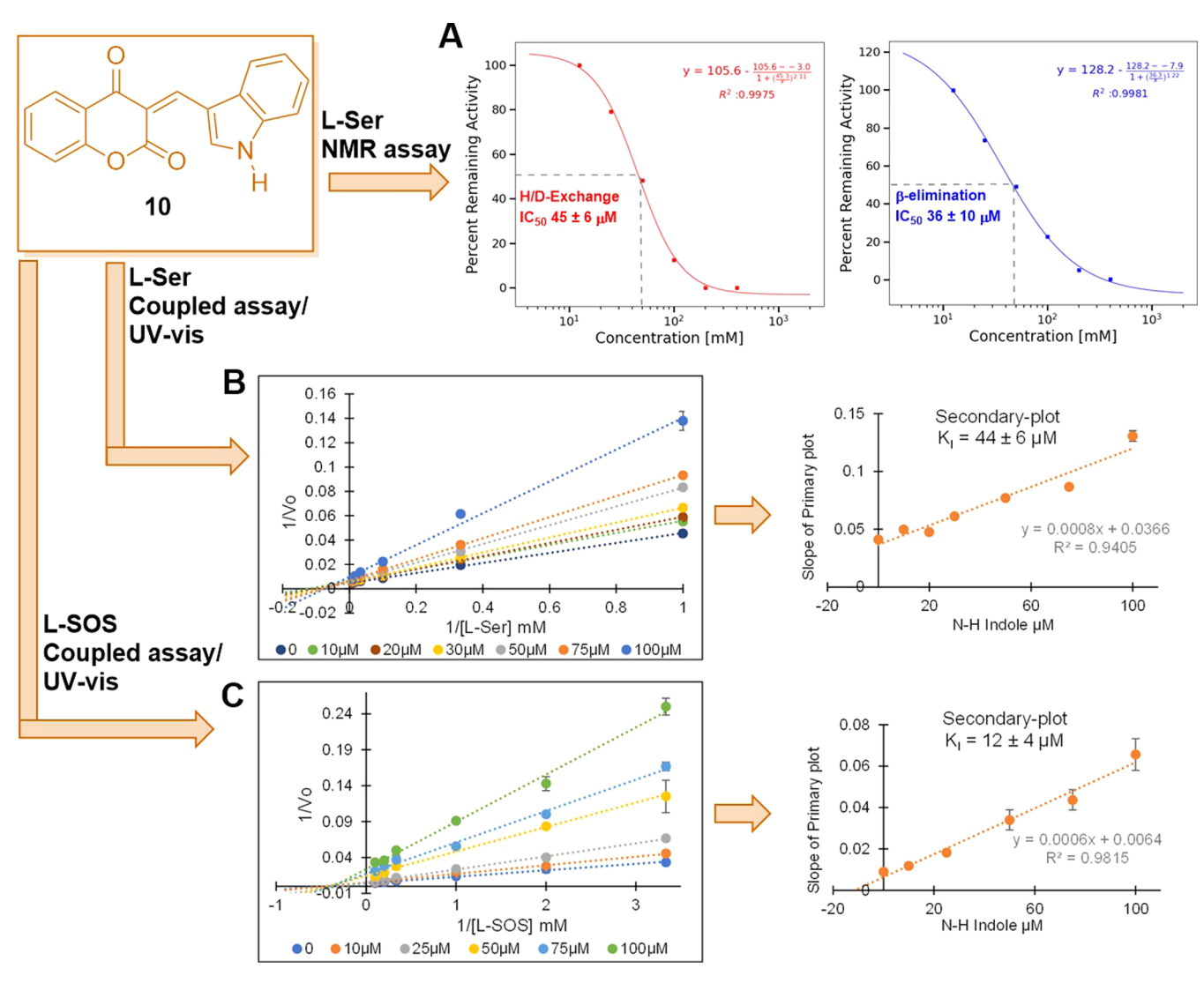


Figure 9. Inhibition profile for N–H indolo-chroman-2,4-dione (10). (A) 13 C– 2 H-isotopic crosstalk NMR assay for hSR inhibition with L-Ser (30 mM), giving IC₅₀(β -elimination) = 36 ± 10 μ M and giving IC₅₀(H/D exchange) = 45 ± 6 μ M, respectively. (B) Steady-state kinetic analysis by coupled, UV–vis assay for β -elimination with L-Ser, giving K_i = 44 ± 6 μ M. (C) Steady-state kinetic analysis by the coupled UV–vis assay for β -elimination with the L-SOS substrate, providing K_i = 12 ± 4 μ M.

well under steady-state kinetic conditions for hSR-mediated L-SOS β -elimination giving $K_i=69\pm16~\mu\mathrm{M}$ and showing a noncompetitive mode of inhibition (Figure S22). To examine SAR in this family, N-alkylated systems 7–9 were tested as well and the data obtained support a noncompetitive inhibition mechanism for this chemotype with K_i values ranging from 11.5 to 92 $\mu\mathrm{M}$ (Figures 7 and S22). The K_i values seemed to generally improve with the reduction of the steric bulk on the nitrogen center of the indole. To test this trend further, we synthesized the simple N–H indolo-chroman-2,4-dione compound (10) directly. We were delighted to see that this compound was both more soluble than the N-alkyl congeners previously studied and a more potent hSR inhibitor, showing complete inhibition at 1 mM under ¹³C NMR assay conditions.

Compound 10 was next subjected to complete IC₅₀ analysis with the new $^{13}\text{C}-^2\text{H}$ -isotopic crosstalk assay for hSR inhibition, yielding IC₅₀(H/D-exchange) = 45 \pm 6 μ M and IC₅₀(β -elimination) = 36 \pm 10 μ M (Figure 9A). Follow-on comprehensive steady-state kinetic analysis for hSR-mediated β -elimination of L-Ser and L-SOS gave, respectively, K_i (L-Ser

elim) = $44 \pm 6 \,\mu\text{M}$ (Figure 9B) and $K_{\rm i}$ (L-SOS elim) = $12 \pm 4 \,\mu\text{M}$ (Figure 9C). Both assays evidence clear noncompetitive inhibition, as with all other members of this indolo-chroman-2,4-dione family synthesized and investigated here. This suggests that this new family of inhibitors may be binding to the allosteric, ATP-binding site. In fact, in pioneering work, Mozzarelli and co-workers showed that nicotinamide mononucleotide, reduced form (NMNH), exhibits noncompetitive inhibition with respect to the substrate and presumably binds to the ATP-binding pocket of the enzyme. N–H indolo-chroman-2,4-dione 10 displays a $K_{\rm i} = 12 \pm 4 \,\mu\text{M}$ similar to NMNH for which the reported $K_{\rm i} = 18 \pm 7 \,\mu\text{M}$.

Indolo-chroman-2,4-dione System and hSR Binding. In support of the noncompetitive inhibition behavior seen here, a blind-docking exercise suggests that N—H indolo-chroman-2,4-dione (10) binds to the ATP site. It has been demonstrated that there is a critical H-bonding network that connects the ATP site to the active site of the enzyme. These important residues are evident in the 6ZSP structure (Figure 10A). The K279 and N316 are within the hydrogen bonding range of the ribose hydroxyls. R277 hovers over the

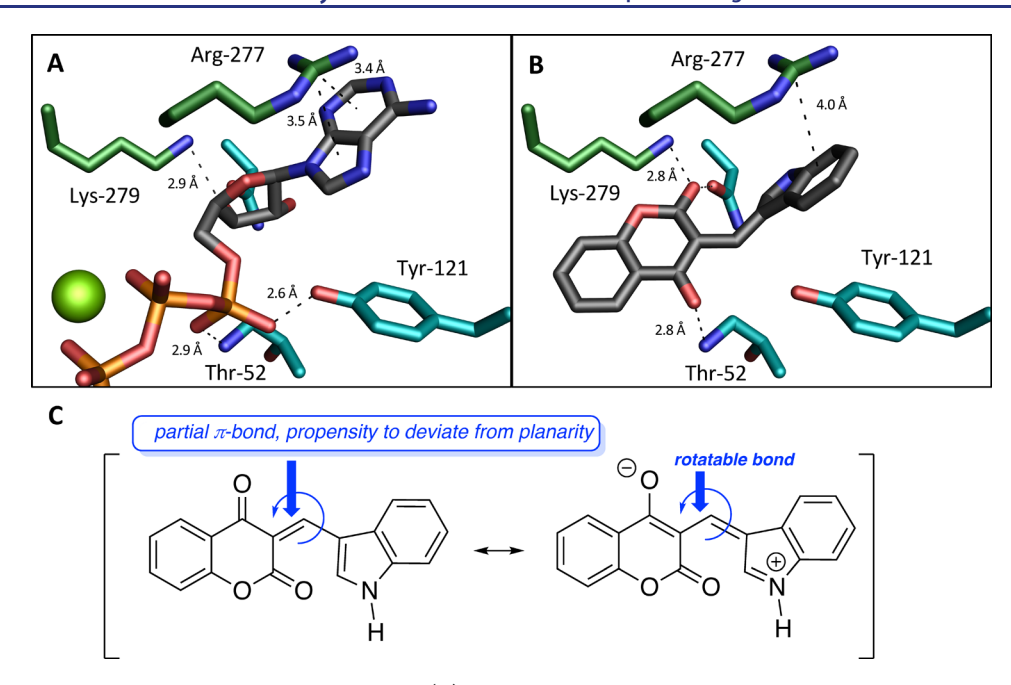


Figure 10. Indolo-chroman-2,4-dione 10 docks to the ATP site. (A) ATP acts in conjunction with a critical, allosteric network linking its binding to the catalytic function at the hSR active site (pdb 6ZSP). (B) Docked structure of N–H indolo-chroman-2,4-dione (10) in the allosteric site of hSR (docking to 6ZSP with the bound-ATP removed) suggests that the indole moiety mimics the adenine ring of ATP. Note that compound 10 bends about the rotatable exomethylene "double bond" upon docking to the ATP site of hSR (autodock FR). (C) Resonance structure picture of compound 10, featuring a partial single bond character about the rotatable bond.

adenine ring allowing for a favorable cation— π interaction with the guanidinium group of arginine. K51 and Y121 anchor in the triphosphate of the ATP.

As can be seen in Figure 10, N-H indolo-chroman-2,4dione 10 finds its way into the ATP site, and in so doing evidences an apparent inherent malleability for this chemotype. Resonance structure analysis (Figure 10C) suggests that the exomethylene "double bond" in the chroman-2,4-dione form should only confer a partial double bond character to the system, as a significant contribution to the hybrid from the oxido-coumarin resonance form is expected. Preliminary modeling results are consistent with this notion. Thus, an initial geometry optimization was performed on 10 using density functional theory (DFT) methods (B3LYP; 6-31G* basis set). To estimate the barrier to rotation around the exomethylene π -bond, a profile scan of 24 dihedral angles incremented every 15° was run using an expanded basis set (6-311G(d,p)). One obtains a rotational barrier of 14.0 kcal/mol about this bond, prompting us to set this as a rotatable bond for the molecular docking to the hSR protein (pdp 6ZSP;^{31a} ATP removed).

In fact, in the course of the molecular docking, compound 10 bends about the exomethylene bond by 70° (Figure 10B) reproducibly docking to the allosteric site in a very similar manner to the native ATP ligand itself (Figure 10A). Of particular note, the indole ring in 10 appears to dock well to the adenine pocket, retaining the favorable cation— π interaction with R277⁵⁶ seen in the ATP-hSR crystal structure. The fact that we observe a Hill coefficient \sim 2 in the dose–response curve for compound 10 in the NMR assay (Figure 9A) is indicative of a high level of cooperativity in inhibitor binding to the native hSR dimer, consistent with its binding to the ATP site at the dimer interface.

To test this idea further, compound 10 was competed against ATP, under steady-state conditions with hSR, holding

the L-Ser concentration constant at 30 mM. One sees an inhibition pattern consistent with compound 10 competing with ATP for the allosteric site (see Figure S24). Importantly, this N–H indolo-chroman-2,4-dione chemotype also has a favorable Lipinski profile, including possessing three H-bond acceptors, one H-bond donor, $clog_p < 5$, and a topological polar surface area estimated to be 59.2. All in all, the experimental observations and modeling results reported here are quite promising and auger well for future efforts to both build around this "hit" result.

CONCLUSIONS AND GENERALIZABILITY

The title enzyme, human serine racemase (hSR), is the only bona fide PLP-dependent amino acid racemase known in human biology, converting L-Ser to D-Ser. Whereas D-amino acids used to be considered the domain of bacterial biology, we now know that D-Ser is a critical neuronal signaling molecule in human biology, serving as the principal coagonist of the NMDA receptor (NMDAR). Normal D-Ser signaling at the NMDAR is essential for long-term potentiation (LTP) associated with learning and memory. 10a,b On the other hand, hSR hyperfunction is associated with Alzheimer's disease, 18 ALS, 21 and neuronal infarction pursuant to ischemic stroke, 25 whereas hSR hypofunction correlates with schizophrenia.⁵⁷ Moreover, recent work indicates that the second hSR function, namely, β -elimination of L-Ser to pyruvate, and thence acetyl-CoA, is a hallmark of colorectal cancer, leading to elevated metabolism and acetylation of histone H3.

Against the backdrop of this remarkable biology, there is widespread interest in both developing new tools to measure hSR activity and developing new inhibitors for the enzyme as tools for chemical biology. The title assay does both, directly measuring both the α -deprotonation chemistry associated with the racemization function and the β -elimination function associated with pyruvate formation. The assay utilizes only the

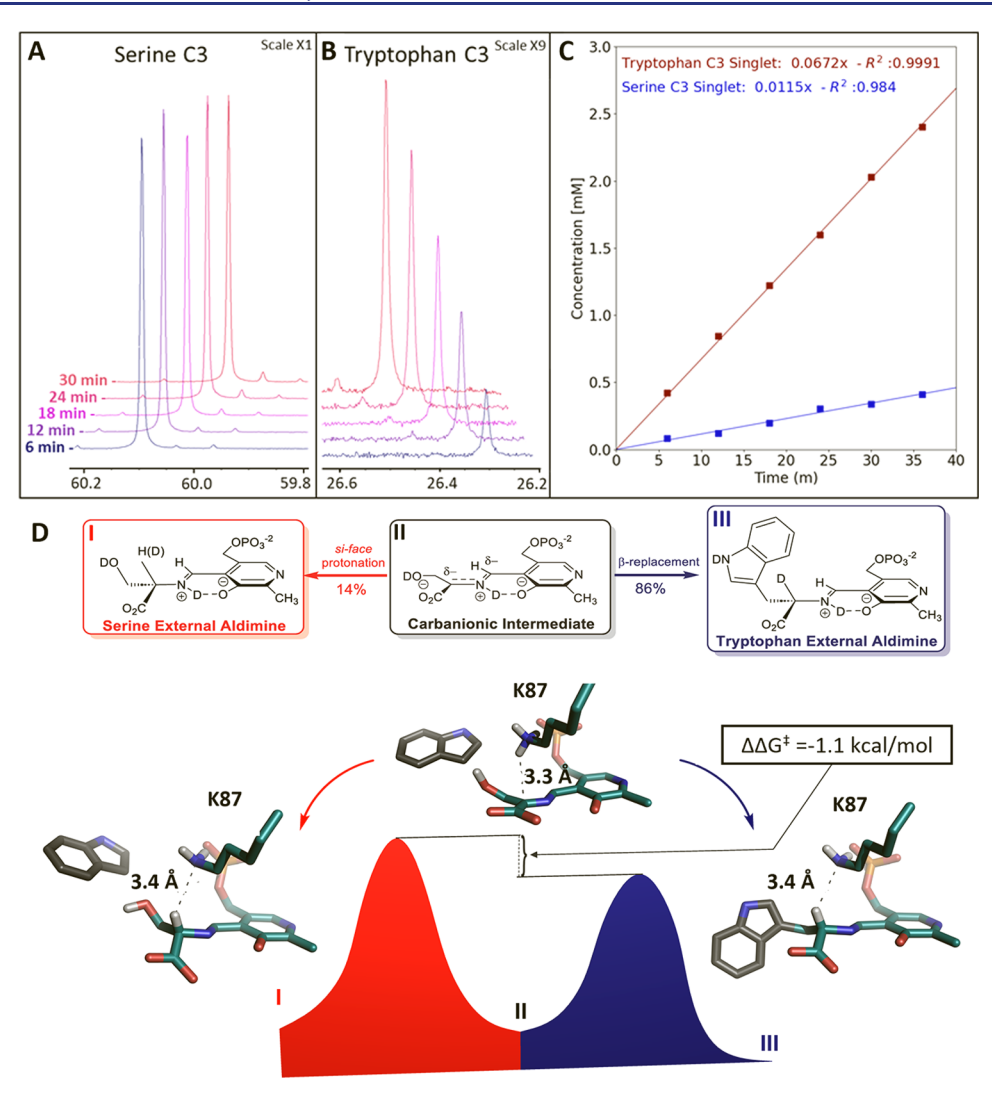


Figure 11. 13 C/ 2 H NMR crosstalk assay for *Salmonella typhimurium* tryptophan synthase. Experiments showing the application this isotopic crosstalk assay to another enzyme, tryptophan synthase (TS), within the same fold-type II PLP enzyme superfamily. The assay utilizes 30 mM L-Ser labeled equally at C2 and C3 with 13 C (segregated isotopic labeling@15 mM each) and 20 mM indole in 100 mM TEA buffer, pD = 8 containing 10% DMSO, 50 mM KCl. Once again, crisp time points were obtained by quenching with aminooxyacetic acid (275 mM) every 5 min. (A) 13 C NMR stack plot (700 MHz NMR; 175 MHz for 13 C) of the 13 C-enriched serine C3 peak, showing the appearance of the upfield-shifted peak (~60.05 ppm) corresponding to L-Ser-deuteration at C2. (B) Emergence of a new peak corresponding to C3 of L-tryptophan is indicative of the β-replacement reaction. (C) Time-point assay plot with TS using this assay. Note that the β-replacement is favored ~6-fold over carbanionic intermediate reprotonation (H/D exchange). (D) Free energy diagram showing the "partitioning fingerprint" for the carbanionic intermediate in TS. The coordinates of the TS carbanionic intermediate shown above (II) were imported from pdb 4HPJ. The atoms of the artificial nucleophile, ρ-aminophenol, have been deleted and replaced with an OH to model the Ser substrate. The external aldimines for L-Ser (substrate) and L-Trp (product) were modeled beginning from the coordinates of this structure as well.

native enzyme and the native substrate. There is no need to use a coupling enzyme or to install a chromophore. The assay is used here to screen a library of 1020 inhibitor candidates and identifies an interesting family of indolo-chroman-2,4-diones that bind as well as any inhibitor yet described. Kinetic analysis (noncompetitive inhibition vs L-Ser substrate; competitive inhibition vs ATP) and molecular docking suggest that these compounds are hitting the interesting allosteric, ATP-binding pocket.

Finally, this new ¹³C/²H isotopic crosstalk NMR assay is expected to be broadly applicable. As a forward-looking test of this, we have expressed, purified, and characterized another PLP enzyme, tryptophan synthase (TS), and deployed the assay in this active site (see the SI for full details). As is illustrated in Figure 11, in the presence of imidazole and L-

serine (featuring segregated C2, C3 $^{-13}$ C-labeling as for the hSR assay) one obtains sharp initial rates for both the β -replacement reaction characteristic of this enzyme and for siface reprotonation (deuteration here). Note the dramatically different partition ratio in the TS active site (β -replacement/siface protonation \sim 6:1) vs that seen with hSR (β -elimination/si-face protonation \sim 1:3.6—see Figure 4). This difference in internal free energy landscapes is quite striking given that hSR and TS share important common active site characteristics and are members of the same enzymatic superfamily [fold-type II; Ser-residue opposite the pyridine N in the PLP binding site (S313 in hSR; S177 in TS); aromatic residue engaged in an edge-to-face π - π interaction with the PLP ring (F55 in hSR; H86 in TS)]. These results also highlight the novelty and importance of the si-face protonation window for measuring

hSR active site chemistry, a window not previously observed prior to this report.

In summary, from the point of view of chemical biology, the title assay provides a new NMR-based window through which experimentalists can screen different activities of PLP enzymes in parallel to aid in the important search for small-molecule effectors. From the point of view of mechanistic enzymology, this assay delivers a diagnostic NMR-based PLP-carbanion "partitioning fingerprint" that reveals nuanced but distinctive and important features of the free energy profile surrounding this ubiquitous, yet elusive intermediate in PLP enzyme active sites.

ASSOCIATED CONTENT

5 Supporting Information

The Supporting Information is available free of charge at https://pubs.acs.org/doi/10.1021/jacs.2c12774.

Detailed experimental procedures for NMR assay development and deployment in both the hSR and TS active sites and purification/characterization of both enzymes; independent kinetic characterization of "hit" compounds; complete library description; and heat maps of all compounds screened; and synthetic details and spectral data for all new compounds (PDF)

Animation illustrating both the favored *si*-face over *re*-face protonation and the postulated *re*-face proton shuttle (MOV)

AUTHOR INFORMATION

Corresponding Author

David B. Berkowitz — Department of Chemistry, University of Nebraska, Lincoln, Lincoln, Nebraska 68588, United States; orcid.org/0000-0001-7550-0112; Phone: +1 402 472 2738; Email: dberkowitz1@unl.edu; Fax: +1 402 472 9402

Authors

Stephany M. Ramos de Dios — Department of Chemistry, University of Nebraska, Lincoln, Lincoln, Nebraska 68588, United States; Present Address: Biogen, Durham, North Carolina 27709, United States; orcid.org/0000-0001-7174-7142

Jared L. Hass – Department of Chemistry, University of Nebraska, Lincoln, Lincoln, Nebraska 68588, United States; orcid.org/0000-0002-0903-6291

Danielle L. Graham — Department of Chemistry, University of Nebraska, Lincoln, Lincoln, Nebraska 68588, United States; Present Address: Northrup Grunman Innovation Systems, Magna, Utah 84044, United States.; orcid.org/0000-0003-2922-6268

Nivesh Kumar — Department of Chemistry, University of Nebraska, Lincoln, Lincoln, Nebraska 68588, United States; orcid.org/0000-0003-3723-6642

Aina E. Antony — Department of Chemistry, University of Nebraska, Lincoln, Lincoln, Nebraska 68588, United States; orcid.org/0000-0002-4008-8081

Martha D. Morton – Department of Chemistry, University of Nebraska, Lincoln, Lincoln, Nebraska 68588, United States; orcid.org/0000-0002-6411-1733

Complete contact information is available at: https://pubs.acs.org/10.1021/jacs.2c12774

Author Contributions

§S.M.R.d.D., J.L.H., and D.L.G. contributed equally to this work.

Notes

The authors declare no competing financial interest.

ACKNOWLEDGMENTS

The authors thank the NSF (CHE/CBET-2102705) and the University of Nebraska College of Arts & Sciences for support. Cambridge Isotope Laboratories is acknowledged for a minigrant in support of these studies. These studies were facilitated by the IR/D (Individual Research and Development) Program associated with DBB's appointment at the National Science Foundation. The authors thank the NIH (SIG-1-510-RR-06307) and NSF (CHE-0091975, MRI-0079750) for NMR instrumentation support and the NIH (RR016544) for research facilities. A helium recovery system supporting the 700 MHz NMR instrument was purchased with support from the NCIBC Systems Biology Core (NIH NIGMS P20 GM113126). Tzanko Doukov (Stanford University) and David L. Nelson and Ranjeet A. Dhokale (both U. Nebraska co-workers) are thanked for their helpful discussions.

DEDICATION

This manuscript is dedicated to the memory of Christopher T. Walsh for his inspirational pioneering work on the molecular mechanisms of PLP enzymes.

REFERENCES

- (1) Fux, A.; Pfanzelt, M.; Kirsch, V. C.; Hoegl, A.; Sieber, S. A. Customizing functionalized cofactor mimics to study the human pyridoxal 5'-phosphate-binding proteome. *Cell Chem. Biol.* **2019**, *26*, 1461.e7–1468.e7.
- (2) Percudani, R.; Peracchi, A. A genomic overview of pyridoxal-phosphate-dependent enzymes. *EMBO Rep.* **2003**, *4*, 850–854.
- (3) (a) Grishin, N. V.; Osterman, A. L.; Brooks, H. B.; Phillips, M. A.; Goldsmith, E. J. X-ray structure of ornithine decarboxylase from *Trypanosoma brucei*: The native structure and the structure in complex with α -difluoromethylornithine. *Biochemistry* **1999**, *38*, 15174–15184. (b) Jackson, L. K.; Goldsmith, E. J.; Phillips, M. A. X-ray structure determination of *Trypanosoma brucei* ornithine decarboxylase bound to D-ornithine and to G418. Insights into substrate binding and ODC conformational flexibility. *J. Biol. Chem.* **2003**, *278*, 22037–22043.
- (4) Burkhard, P.; Dominici, P.; Borri-Voltattorni, C.; Jansonius, J. N.; Malashkevich, V. N. Structural insight into Parkinson's disease treatment from drug-inhibited DOPA decarboxylase. *Nat. Struct. Biol.* **2001**, *8*, 963–967.
- (5) (a) Shen, S.; Doubleday, P. F.; Weerawarna, P. M.; Zhu, W.; Kelleher, N. L.; Silverman, R. B. Mechanism-based design of 3-amino-4-halocyclopentenecarboxylic acids as inactivators of GABA aminotransferase. ACS Med. Chem. Lett. 2020, 11, 1949-1955. (b) Juncosa, J. I.; Takaya, K.; Le, H. V.; Moschitto, M. J.; Weerawarna, P. M.; Mascarenhas, R.; Liu, D.; Dewey, S. L.; Silverman, R. B. Design and mechanism of (S)-3-amino-4-(difluoromethylenyl)cyclopent-1-ene-1carboxylic acid, a highly potent γ -aminobutyric acid aminotransferase inactivator for the treatment of addiction. J. Am. Chem. Soc. 2018, 140, 2151-2164. (c) Liu, W.; Peterson Peter, E.; Carter Richard, J.; Zhou, X.; Langston James, A.; Fisher Andrew, J.; Toney Michael, D. Crystal structures of unbound and aminooxyacetate-bound Escherichia coli gamma-aminobutyrate aminotransferase. Biochemistry 2004, 43, 10896-10905. (d) Choi, S.; Storici, P.; Schirmer, T.; Silverman, R. B. Design of a conformationally restricted analog of the antiepilepsy drug vigabatrin that directs its mechanism of inactivation of γ aminobutyric acid aminotransferase. J. Am. Chem. Soc. 2002, 124, 1620-1624.

- (6) (a) Silverman, R. B. Inactivators of ornithine aminotransferase for the treatment of hepatocellular carcinoma. ACS Med. Chem. Lett. 2022, 13, 38-49. (b) Zhu, W.; Doubleday, P. F.; Butrin, A.; Weerawarna, P. M.; Melani, R. D.; Catlin, D. S.; Dwight, T. A.; Liu, D.; Kelleher, N. L.; Silverman, R. B. Remarkable and unexpected mechanism for (S)-3-amino-4-(difluoromethylenyl)cyclohex-1-ene-1carboxylic acid as a selective inactivator of human ornithine aminotransferase. J. Am. Chem. Soc. 2021, 143, 8193-8207. (c) Shen, S.; Butrin, A.; Doubleday, P. F.; Melani, R. D.; Beaupre, B. A.; Tavares, M. T.; Ferreira, G. M.; Kelleher, N. L.; Moran, G. R.; Liu, D.; Silverman, R. B. Turnover and inactivation mechanisms for (S)-3-amino-4,4-difluorocyclopent-1-enecarboxylic acid, a selective mechanism-based inactivator of human ornithine aminotransferase. J. Am. Chem. Soc. 2021, 143, 8689-8703. (d) Butrin, A.; Beaupre, B. A.; Kadamandla, N.; Zhao, P.; Shen, S.; Silverman, R. B.; Moran, G. R.; Liu, D. Structural and kinetic analyses reveal the dual inhibition modes of ornithine aminotransferase by (15,3S)-3-amino-4-(hexafluoropropan-2-ylidenyl)-cyclopentane-1-carboxylic acid (BCF₃). ACS Chem. Biol. 2021, 16, 67-75. (e) Zhu, W.; Doubleday, P. F.; Catlin, D. S.; Weerawarna, P. M.; Butrin, A.; Shen, S.; Wawrzak, Z.; Kelleher, N. L.; Liu, D.; Silverman, R. B. A remarkable difference that one fluorine atom confers on the mechanisms of inactivation of human ornithine aminotransferase by two cyclohexene analogues of γ aminobutyric acid. J. Am. Chem. Soc. 2020, 142, 4892-4903.
- (7) Li, B.; Deng, X.; Kim, S. H.; Buhrow, L.; Tomchick, D. R.; Phillips, M. A.; Michael, A. J. Alternative pathways utilize or circumvent putrescine for biosynthesis of putrescine-containing rhizoferrin. *J. Biol. Chem.* **2021**, 296, No. 100146.
- (8) Maenpuen, S.; Sopitthummakhun, K.; Yuthavong, Y.; Chaiyen, P.; Leartsakulpanich, U. Characterization of *Plasmodium falciparum* serine hydroxymethyltransferase-a potential antimalarial target. *Mol. Biochem. Parasitol.* **2009**, *168*, 63–73.
- (9) (a) McCune, C. D.; Chan, S. J.; Beio, M. L.; Shen, W.; Chung, W. J.; Szczesniak, L. M.; Chai, C.; Koh, S. Q.; Wong, P. T. H.; Berkowitz, D. B. "Zipped synthesis" by cross-metathesis provides a cystathionine β -synthase inhibitor that attenuates cellular H₂S levels and reduces neuronal infarction in a rat ischemic stroke model. ACS Cent. Sci. 2016, 2, 242–252. (b) Koutmos, M.; Kabil, O.; Smith, J. L.; Banerjee, R. Structural basis for substrate activation and regulation by cystathionine beta-synthase (cbs) domains in cystathionine β -synthase. Proc. Natl. Acad. Sci. U.S.A. 2010, 107, 20958–20963.
- (10) (a) Graham, D. L.; Beio, M. L.; Nelson, D. L.; Berkowitz, D. B. Human serine racemase: Key residues/active site motifs and their relation to enzyme function. Front. Mol. Biosci. 2019, 6, No. 8. (b) Raboni, S.; Marchetti, M.; Faggiano, S.; Campanini, B.; Bruno, S.; Marchesani, F.; Margiotta, M.; Mozzarelli, A. The energy landscape of human serine racemase. Front. Mol. Biosci. 2019, 5, No. 112. (c) Ishiwata, S.; Umino, A.; Balu, D. T.; Coyle, J. T.; Nishikawa, T. Neuronal serine racemase regulates extracellular D-serine levels in the adult mouse hippocampus. J. Neural Transm. 2015, 122, 1099-1103. (d) Balu, D. T.; Takagi, S.; Puhl, M. D.; Benneyworth, M. A.; Coyle, J. T. D-Serine and serine racemase are localized to neurons in the adult mouse and human forebrain. Cell. Mol. Neurobiol. 2014, 34, 419-435. (e) Hoffman, H. E.; Jiraskova, J.; Ingr, M.; Zvelebil, M.; Konvalinka, J. Recombinant human serine racemase: Enzymologic characterization and comparison with its mouse ortholog. Protein Expression Purif. 2009, 63, 62-67. (f) De Miranda, J.; Santoro, A.; Engelender, S.; Wolosker, H. Human serine racemase: Molecular cloning, genomic organization and functional analysis. Gene 2000, 256, 183-188. (g) Wolosker, H.; Blackshaw, S.; Snyder, S. H. Serine racemase: A glial enzyme synthesizing D-serine to regulate glutamate-N-methyl-Daspartate neurotransmission. Proc. Natl. Acad. Sci. U.S.A. 1999, 96, 13409-13414.
- (11) (a) Takagi, S.; Puhl, M. D.; Anderson, T.; Balu, D. T.; Coyle, J. T. Serine racemase expression by striatal neurons. *Cell. Mol. Neurobiol.* **2022**, *42*, 279–289. (b) Wolosker, H.; Balu, D. T. D-Serine as the gatekeeper of NMDA receptor activity: Implications for the pharmacologic management of anxiety disorders. *Transl. Psychiatry* **2020**, *10*, No. 184. (c) Bodner, O.; Radzishevsky, I.; Foltyn, V. N.;

- Touitou, A.; Valenta, A. C.; Rangel, I. F.; Panizzutti, R.; Kennedy, R. T.; Billard, J. M.; Wolosker, H. D-Serine signaling and nmdarmediated synaptic plasticity are regulated by system a-type of glutamine/D-serine dual transporters. J. Neurosci. 2020, 40, 6489-6502. (d) Neame, S.; Safory, H.; Radzishevsky, I.; Touitou, A.; Marchesani, F.; Marchetti, M.; Kellner, S.; Berlin, S.; Foltyn, V. N.; Engelender, S.; Billard, J.-M.; Wolosker, H. The NMDA receptor activation by D-serine and glycine is controlled by an astrocytic PHGDH-dependent serine shuttle. Proc. Natl. Acad. Sci. U.S.A. 2019, 116, 20736-20742. (e) Wolosker, H. The neurobiology of D-serine signaling. Adv. Pharmacol. 2018, 82, 325-348. (f) Meunier, C. N. J.; Dallerac, G.; Le Roux, N.; Sacchi, S.; Levasseur, G.; Amar, M.; Pollegioni, L.; Mothet, J. P.; Fossier, P. D-Serine and glycine differentially control neurotransmission during visual cortex critical period. PLoS One 2016, 11, No. e0151233. (g) Wolosker, H.; Radzishevsky, I. The serine shuttle between glia and neurons: Implications for neurotransmission and neurodegeneration. Biochem. Soc. Trans. 2013, 41, 1546-1550. (h) Wolosker, H.; Dumin, E.; Balan, L.; Foltyn, V. N. D-Amino acids in the brain: D-serine in neurotransmission and neurodegeneration. FEBS J. 2008, 275, 3514-3526. (i) Baumgart, F.; Rodriguez-Crespo, I. D-Amino acids in the brain: The biochemistry of brain serine racemase. FEBS J. 2008, 275, 3538–3545. (j) Boehning, D.; Snyder, S. H. Novel neural modulators. Annu. Rev. Neurosci. 2003, 26, 105-131. (k) Mothet, J.-P.; Parent, A. T.; Wolosker, H.; Brady, R. O., Jr.; Linden, D. J.; Ferris, C. D.; Rogawski, M. A.; Snyder, S. H. D-Serine is an endogenous ligand for the glycine site of the N-methyl-D-aspartate receptor. Proc. Natl. Acad. Sci. U.S.A. 2000, 97, 4926-4931.
- (12) Furukawa, H.; Gouaux, E. Mechanisms of activation, inhibition and specificity: Crystal structures of the NMDA receptor NR1 ligand-binding core. *EMBO J.* **2003**, *22*, 2873–2885.
- (13) Berger, A. J.; Dieudonne, S.; Ascher, P. Glycine uptake governs glycine site occupancy at NMDA receptors of excitatory synapses. *J. Neurophysiol.* **1998**, *80*, 3336–3340.
- (14) Ploux, E.; Bouet, V.; Radzishevsky, I.; Wolosker, H.; Freret, T.; Billard, J.-M. Serine racemase deletion affects the excitatory/inhibitory balance of the hippocampal cal network. *Int. J. Mol. Sci.* **2020**, *21*, No. 9447
- (15) Wolosker, H. NMDA receptor regulation by p-serine: New findings and perspectives. *Mol. Neurobiol.* **2007**, *36*, 152–164.
- (16) Balu, D. T.; Coyle, J. T. Altered CREB binding to activity-dependent genes in serine racemase deficient mice, a mouse model of schizophrenia. ACS Chem. Neurosci. 2018, 9, 2205–2209.
- (17) Mustafa, A. K.; Ahmad, A. S.; Zeynalov, E.; Gazi, S. K.; Sikka, G.; Ehmsen, J. T.; Barrow, R. K.; Coyle, J. T.; Snyder, S. H.; Dore, S. Serine racemase deletion protects against cerebral ischemia and excitotoxicity. *J. Neurosci.* **2010**, *30*, 1413–1416.
- (18) Balu, D. T.; Pantazopoulos, H.; Huang, C. C. Y.; Muszynski, K.; Harvey, T. L.; Uno, Y.; Rorobaugh, J. M.; Galloway, C. R.; Botz-Zapp, C.; Berretta, S.; Weinshenker, D.; Coyle, J. T. Neurotoxic astrocytes express the D-serine synthesizing enzyme, serine racemase, in Alzheimer's disease. *Neurobiol. Dis.* **2019**, *130*, No. 104511.
- (19) Inoue, R.; Hashimoto, K.; Harai, T.; Mori, H. NMDA- and β -amyloid1-42-induced neurotoxicity is attenuated in serine racemase knock-out mice. *J. Neurosci.* **2008**, 28, 14486–14491.
- (20) Madeira, C.; Lourenco, M. V.; Vargas-Lopes, C.; Suemoto, C. K.; Brandao, C. O.; Reis, T.; Leite, R. E. P.; Laks, J.; Jacob-Filho, W.; Pasqualucci, C. A.; Grinberg, L. T.; Ferreira, S. T.; Panizzutti, R. D-Serine levels in Alzheimer's disease: Implications for novel biomarker development. *Transl. Psychiatry* **2015**, *5*, No. e561.
- (21) Paul, P.; de Belleroche, J. The role of D-serine and glycine as coagonists of NMDA receptors in motor neuron degeneration and amyotrophic lateral sclerosis (ALS). Front. Synaptic Neurosci. 2014, 6, No. 10.
- (22) Lefèvre, Y.; Amadio, A.; Vincent, P.; Descheemaeker, A.; Oliet, S. H. R.; Dallel, R.; Voisin, D. L. Neuropathic pain depends upon Deserine co-activation of spinal NMDA receptors in rats. *Neurosci. Lett.* **2015**, *603*, 42–47.

- (23) Dong, C.; Zhang, J.-C.; Ren, Q.; Ma, M.; Qu, Y.; Zhang, K.; Yao, W.; Ishima, T.; Mori, H.; Hashimoto, K. Deletion of serine racemase confers D-serine -dependent resilience to chronic social defeat stress. *Neurochem. Int.* **2018**, *116*, 43–51.
- (24) Balu, D. T.; Presti, K. T.; Huang, C. C. Y.; Muszynski, K.; Radzishevsky, I.; Wolosker, H.; Guffanti, G.; Ressler, K. J.; Coyle, J. T. Serine racemase and D-serine in the amygdala are dynamically involved in fear learning. *Biol. Psychiatry* **2018**, *83*, 273–283.
- (25) Tapanes, S. A.; Arizanovska, D.; Díaz, M. M.; Folorunso, O. O.; Harvey, T.; Brown, S. E.; Radzishevsky, I.; Close, L. N.; Jagid, J. R.; Cordeiro, J. G.; Wolosker, G.; Balu, D. T.; Liebl, D. J. Inhibition of glial D-serine release rescues synaptic damage after brain injury. *Glia* 2022, 70, 1133–1152.
- (26) Nelson, D. L.; Applegate, G. A.; Beio, M. L.; Graham, D. L.; Berkowitz, D. B. Human serine racemase structure/activity relationship studies provide mechanistic insight and point to position 84 as a hot spot for β -elimination function. *J. Biol. Chem.* **2017**, 292, 13986–14002
- (27) Foltyn, V. N.; Bendikov, I.; De Miranda, J.; Panizzutti, R.; Dumin, E.; Shleper, M.; Li, P.; Toney, M. D.; Kartvelishvily, E.; Wolosker, H. Serine racemase modulates intracellular D-serine levels through an α,β -elimination activity. *J. Biol. Chem.* **2005**, 280, 1754–1763.
- (28) Ohshima, K.; Nojima, S.; Tahara, S.; Kurashige, M.; Kawasaki, K.; Hori, Y.; Taniguchi, M.; Umakoshi, Y.; Okuzaki, D.; Wada, N.; Ikeda, J.-i.; Fukusaki, E.; Morii, E. Serine racemase enhances growth of colorectal cancer by producing pyruvate from serine. *Nat. Metab.* **2020**, *2*, 81–96.
- (29) Di Cerbo, V.; Mohn, F.; Ryan, D. P.; Montellier, E.; Kacem, S.; Tropberger, P.; Kallis, E.; Holzner, M.; Hoerner, L.; Feldmann, A.; Richter, F. M.; Bannister, A. J.; Mittler, G.; Michaelis, J.; Khochbin, S.; Feil, R.; Schuebeler, D.; Owen-Hughes, T.; Daujat, S.; Schneider, R. Acetylation of histone H3 at lysine 64 regulates nucleosome dynamics and facilitates transcription. *eLife* **2014**, *3*, No. e01632.
- (30) Cui, Z.; Mo, J.; Wang, L.; Wang, R.; Cheng, F.; Wang, L.; Yang, X.; Wang, W. Integrated bioinformatics analysis of serine racemase as an independent prognostic biomarker in endometrial cancer. *Front. Genet.* **2022**, *13*, No. 906291.
- (31) (a) Koulouris, C. R.; Gardiner, S. E.; Harris, T. K.; Elvers, K. T.; Mark Roe, S.; Gillespie, J. A.; Ward, S. E.; Grubisha, O.; Nicholls, R. A.; Atack, J. R.; Bax, B. D. Tyrosine 121 moves revealing a ligandable pocket that couples catalysis to ATP-binding in serine racemase. Commun. Biol. 2022, 5, No. 346. (b) Michielon, A.; Marchesani, F.; Faggiano, S.; Giaccari, R.; Campanini, B.; Bettati, S.; Mozzarelli, A.; Bruno, S. Human serine racemase is inhibited by glyceraldehyde 3-phosphate, but not by glyceraldehyde 3-phosphate dehydrogenase. Biochim. Biophys. Acta, Proteins Proteomics 2021, 1869, No. 140544. (c) Rani, K.; Tyagi, M.; Mazumder, M.; Singh, A.; Shanmugam, A.; Dalal, K.; Pillai, M.; Samudrala, G.; Kumar, S.; Srinivasan, A. Accelerated identification of serine racemase inhibitor from Centella asiatica. Sci. Rep. 2020, 10, No. 4640. (d) Mori, H.; Wada, R.; Takahara, S.; Horino, Y.; Izumi, H.; Ishimoto, T.; Yoshida, T.; Mizuguchi, M.; Obita, T.; Gouda, H.; Hirono, S.; Toyooka, N. A novel serine racemase inhibitor suppresses neuronal over-activation in vivo. Bioorg. Med. Chem. 2017, 25, 3736-3745. (e) Foster, A. C.; Li, Y.-X.; Runyan, S.; Dinh, T.; Venadas, S.; Chen, J.; Pashikanti, S.; Datta, A.; Ehring, G.; Staubli, U. Activity of the enantiomers of erythro-3-hydroxyaspartate at glutamate transporters and NMDA receptors. J. Neurochem. 2016, 136, 692-697. (f) Bruno, S.; Marchesani, F.; Dellafiora, L.; Margiotta, M.; Faggiano, S.; Campanini, B.; Mozzarelli, A. Human serine racemase is allosterically modulated by NADH and reduced nicotinamide derivatives. Biochem. J. 2016, 473, 3505-3516. (g) Beato, C.; Pecchini, C.; Cocconcelli, C.; Campanini, B.; Marchetti, M.; Pieroni, M.; Mozzarelli, A.; Costantino, G. Cyclopropane derivatives as potential human serine racemase inhibitors: Unveiling novel insights into a difficult target. J. Enzyme Inhib. Med. Chem. 2016, 31, 645-652.
- (32) (a) McCune, C. D.; Beio, M. L.; Sturdivant, J. M.; de la Salud-Bea, R.; Darnell, B. M.; Berkowitz, D. B. Synthesis and deployment of

- an elusive fluorovinyl cation equivalent: Access to quaternary α -(1'fluoro) vinyl amino acids as potential PLP enzyme inactivators. J. Am. Chem. Soc. 2017, 139, 14077-14089. (b) Berkowitz, D. B.; Karukurichi, K. R.; de la Salud-Bea, R.; Nelson, D. L.; McCune, C. D. Use of fluorinated functionality in enzyme inhibitor development: Mechanistic and analytical advantages. J. Fluorine Chem. 2008, 129, 731-742. (c) Karukurichi, K. R.; de la Salud-Bea, R.; Jahng, W. J.; Berkowitz, D. B. Examination of the new α -(2'Z-fluoro)vinyl trigger with lysine decarboxylase: The absolute stereochemistry dictates the reaction course. J. Am. Chem. Soc. 2007, 129, 258-259. (d) Berkowitz, D. B.; Wu, B.; Li, H. A formal [3, 3]-sigmatropic rearrangement route to quaternary α -vinyl amino acids: Use of allylic N-PMP trifluoroacetimidates. Org. Lett. 2006, 8, 971-974. (e) Berkowitz, D. B.; Maiti, G. Following an ises lead: The first examples of asymmetric Ni(0)-mediated allylic amination. Org. Lett. 2004, 6, 2661-2664. (f) Berkowitz, D. B.; de la Salud-Bea, R.; Jahng, W.-J. Synthesis of quaternary amino acids bearing a (2'Z)-fluorovinyl α branch: Potential PLP enzyme inactivators. Org. Lett. 2004, 6, 1821-1824. (g) Berkowitz, D. B.; Chisowa, E.; McFadden, J. M. Stereocontrolled synthesis of quaternary β , γ -unsaturated amino acids: Chain extension of D- and L- α -(2-tributylstannyl)vinyl amino acids. Tetrahedron 2001, 57, 6329-6343. (h) Berkowitz, D. B.; McFadden, J. M.; Sloss, M. K. Engineering acyclic stereocontrol in the alkylation of vinylglycine-derived dianions: Asymmetric synthesis of higher α -vinyl amino acids. J. Org. Chem. 2000, 65, 2907–2918. (i) Berkowitz, D. B.; McFadden, J. M.; Chisowa, E.; Semerad, C. L. Organoselenium-based entry into versatile, α -(2-tributylstannyl)vinyl amino acids in scalemic form: A new route to vinyl stannanes. J. Am. Chem. Soc. 2000, 122, 11031-11032.
- (33) (a) Stříšovský, K.; Jiraskova, J.; Mikulova, A.; Rulisek, L.; Konvalinka, J. Dual substrate and reaction specificity in mouse serine racemase: Identification of high-affinity dicarboxylate substrate and inhibitors and analysis of the β -eliminase activity. *Biochemistry* **2005**, 44, 13091–13100. (b) Panizzutti, R.; De Miranda, J.; Ribeiro, C. S.; Engelender, S.; Wolosker, H. A new strategy to decrease N-methyl-paspartate (NMDA) receptor coactivation: Inhibition of p-serine synthesis by converting serine racemase into an eliminase. *Proc. Natl. Acad. Sci. U.S.A.* **2001**, 98, 5294–5299.
- (34) Koval, D.; Jiraskova, J.; Strisovsky, K.; Konvalinka, J.; Kasicka, V. Capillary electrophoresis method for determination of D-serine and its application for monitoring of serine racemase activity. *Electrophoresis* **2006**, *27*, 2558–2566.
- (35) Singh, N. S.; Paul, R. K.; Sichler, M.; Moaddel, R.; Bernier, M.; Wainer, I. W. Capillary electrophoresis-laser-induced fluorescence (CE-LIF) assay for measurement of intracellular D-serine and serine racemase activity. *Anal. Biochem.* **2012**, *421*, 460–466.
- (36) Smith, M. A.; Mack, V.; Ebneth, A.; Moraes, I.; Felicetti, B.; Wood, M.; Schonfeld, D.; Mather, O.; Cesura, A.; Barker, J. The structure of mammalian serine racemase: Evidence for conformational changes upon inhibitor binding. *J. Biol. Chem.* **2010**, 285, 12873—12881.
- (37) (a) Dixon, S. M.; Li, P.; Liu, R.; Wolosker, H.; Lam, K. S.; Kurth, M. J.; Toney, M. D. Slow-binding human serine racemase inhibitors from high-throughput screening of combinatorial libraries. *J. Med. Chem.* 2006, 49, 2388–2397. (b) Hoffman, H. E.; Jiraskova, J.; Cigler, P.; Sanda, M.; Schraml, J.; Konvalinka, J. Hydroxamic acids as a novel family of serine racemase inhibitors: Mechanistic analysis reveals different modes of interaction with the pyridoxal-5'-phosphate cofactor. *J. Med. Chem.* 2009, 52, 6032–6041.
- (38) Dajnowicz, S.; Johnston, R. C.; Parks, J. M.; Blakeley, M. P.; Keen, D. A.; Weiss, K. L.; Gerlits, O.; Kovalevsky, A.; Mueser, T. C. Direct visualization of critical hydrogen atoms in a pyridoxal 5'-phosphate enzyme. *Nat. Commun.* **2017**, *8*, No. 955.
- (39) (a) Toney, M. D. Controlling reaction specificity in pyridoxal phosphate enzymes. *Biochim. Biophys. Acta, Proteins Proteomics* **2011**, 1814, 1407–1418. (b) Griswold, W. R.; Toney, M. D. Role of the pyridine nitrogen in pyridoxal 5'-phosphate catalysis: Activity of three classes of plp enzymes reconstituted with deazapyridoxal 5'-phosphate. *J. Am. Chem. Soc.* **2011**, 133, 14823–14830. (c) Griswold,

- W. R.; Fisher, A. J.; Toney, M. D. Crystal structures of aspartate aminotransferase reconstituted with 1-deazapyridoxal 5'-phosphate: Internal aldimine and stable L-aspartate external aldimine. *Biochemistry* **2011**, *50*, 5918–5924. (d) Toney, M. D. Reaction specificity in pyridoxal phosphate enzymes. *Arch. Biochem. Biophys.* **2005**, *433*, 279–287.
- (40) (a) Holmes, J. B.; Liu, V.; Caulkins, B. G.; Hilario, E.; Ghosh, R. K.; Drago, V. N.; Young, R. P.; Romero, J. A.; Gill, A. D.; Bogie, P. M.; Paulino, J.; Wang, X.; Riviere, G.; Bosken, Y. K.; Struppe, J.; Hassan, A.; Guidoulianov, J.; Perrone, B.; Mentink-Vigier, F.; Chang, C.-e. A.; Long, J. R.; Hooley, R. J.; Mueser, T. C.; Dunn, M. F.; Mueller, L. J. Imaging active site chemistry and protonation states: NMR crystallography of the tryptophan synthase α -aminoacrylate intermediate. Proc. Natl. Acad. Sci. U.S.A. 2022, 119, No. e2109235119. (b) Huang, Y.-m. M.; You, W.; Caulkins, B. G.; Dunn, M. F.; Mueller, L. J.; Chang, C.-e. A. Protonation states and catalysis: Molecular dynamics studies of intermediates in tryptophan synthase. Protein Sci. 2016, 25, 166-183. (c) Caulkins, B. G.; Young, R. P.; Kudla, R. A.; Yang, C.; Bittbauer, T. J.; Bastin, B.; Hilario, E.; Fan, L.; Marsella, M. J.; Dunn, M. F.; Mueller, L. J. NMR crystallography of a carbanionic intermediate in tryptophan synthase: Chemical structure, tautomerization, and reaction specificity. J. Am. Chem. Soc. 2016, 138, 15214-15226. (d) Caulkins, B. G.; Bastin, B.; Yang, C.; Neubauer, T. J.; Young, R. P.; Hilario, E.; Huang, Y.-m. M.; Chang, C.-e. A.; Fan, L.; Dunn, M. F.; Marsella, M. J.; Mueller, L. J. Protonation states of the tryptophan synthase internal aldimine active site from solid-state NMR spectroscopy: Direct observation of the protonated Schiff base linkage to pyridoxal-5'-phosphate. J. Am. Chem. Soc. 2014, 136, 12824-12827.
- (41) Nitoker, N.; Major, D. T. Understanding the reaction mechanism and intermediate stabilization in mammalian serine racemase using multiscale quantum-classical simulations. *Biochemistry* **2015**, *54*, 516–527.
- (42) Hanson, K. R.; Rose, I. A. Interpretations of enzyme reaction stereospecificity. *Acc. Chem. Res.* **1975**, *8*, 1–10.
- (43) (a) Xie, X.; Cane, D. E. pH-Rate profiles establish that polyketide synthase dehydratase domains utilize a single-base mechanism. *Org. Biomol. Chem.* **2018**, *16*, 9165–9170. (b) Labonte, J. W.; Townsend, C. A. Active site comparisons and catalytic mechanisms of the hot dog superfamily. *Chem. Rev.* **2013**, *113*, 2182–2204.
- (44) Kumagai, H.; Yamada, H.; Sawada, S.; Schleicher, E.; Mascaro, K.; Floss, H. G. Stereochemistry of the conversion of serine and tyrosine into pyruvate by tyrosine phenol-lyase. *J. Chem. Soc., Chem. Commun.* 1977, 85–86.
- (45) Tsai, M.-D.; Schleicher, E.; Potts, R.; Skye, G. E.; Floss, H. G. Stereochemistry and mechanism of reactions catalyzed by tryptophan synthetase and its $\beta 2$ subunit. *J. Biol. Chem.* **1978**, 253, 5344–5349.
- (46) (a) Vorlová, B.; Nachtigallova, D.; Jiraskova-Vanickova, J.; Ajani, H.; Jansa, P.; Rezac, J.; Fanfrlik, J.; Otyepka, M.; Hobza, P.; Konvalinka, J.; Lepsik, M. Malonate-based inhibitors of mammalian serine racemase: Kinetic characterization and structure-based computational study. Eur. J. Med. Chem. 2015, 89, 189-197. (b) Mori, H.; Wada, R.; Li, J.; Ishimoto, T.; Mizuguchi, M.; Obita, T.; Gouda, H.; Hirono, S.; Toyooka, N. In silico and pharmacological screenings identify novel serine racemase inhibitors. Bioorg. Med. Chem. Lett. 2014, 24, 3732-3735. (c) Harty, M.; Nagar, M.; Atkinson, L.; Le Gay, C. M.; Derksen, D. J.; Bearne, S. L. Inhibition of serine and proline racemases by substrate-product analogues. Bioorg. Med. Chem. Lett. 2014, 24, 390-393. (d) Jiraskova-Vanickova, J.; Ettrich, R.; Vorlova, B.; Hoffman, H. E.; Lepsik, M.; Jansa, P.; Konvalinka, J. Inhibition of human serine racemase, an emerging target for medicinal chemistry. Curr. Drug Targets 2011, 12, 1037-1055.
- (47) Vorlová, B.; Nachtigallová, D.; Jirásková-Vaníčková, J.; Ajani, H.; Jansa, P.; Rezáč, J.; Fanfrlík, J.; Otyepka, M.; Hobza, P.; Konvalinka, J.; Lepšík, M. Malonate-based inhibitors of mammalian serine racemase: Kinetic characterization and structure-based computational study. *Eur. J. Med. Chem.* **2015**, *89*, 189–197.

- (48) Welsch, M. E.; Snyder, S. A.; Stockwell, B. R. Privileged scaffolds for library design and drug discovery. *Curr. Opin. Chem. Biol.* **2010**, *14*, 347–361.
- (49) (a) Grigalunas, M.; Brakmann, S.; Waldmann, H. Chemical evolution of natural product structure. *J. Am. Chem. Soc.* **2022**, *144*, 3314–3329. (b) Karageorgis, G.; Foley, D. J.; Laraia, L.; Waldmann, H. Principle and design of pseudo-natural products. *Nat. Chem.* **2020**, *12*, 227–235. (c) Grigalunas, M.; Burhop, A.; Christoforow, A.; Waldmann, H. Pseudo-natural products and natural product-inspired methods in chemical biology and drug discovery. *Curr. Opin. Chem. Biol.* **2020**, *56*, 111–118. (d) Shang, S.; Tan, D. S. Advancing chemistry and biology through diversity-oriented synthesis of natural product-like libraries. *Curr. Opin. Chem. Biol.* **2005**, *9*, 248–258.
- (50) Christoforow, A.; Wilke, J.; Binici, A.; Pahl, A.; Ostermann, C.; Sievers, S.; Waldmann, H. Design, synthesis, and phenotypic profiling of pyrano-furo-pyridone pseudo natural products. *Angew. Chem., Int. Ed.* **2019**, *58*, 14715–14723.
- (51) (a) Raj, V.; Lee, J. 2H/4H-Chromenes-a versatile biologically attractive scaffold. *Front. Chem.* **2020**, *8*, No. 623. (b) Karageorgis, G.; Reckzeh, E. S.; Ceballos, J.; Schwalfenberg, M.; Sievers, S.; Ostermann, C.; Pahl, A.; Ziegler, S.; Waldmann, H. Chromopynones are pseudo natural product glucose uptake inhibitors targeting glucose transporters glut-1 and -3. *Nat. Chem.* **2018**, *10*, 1103–1111. (c) Keri, R. S.; Budagumpi, S.; Pai, R. K.; Balakrishna, R. G. Chromones as a privileged scaffold in drug discovery: A review. *Eur. J. Med. Chem.* **2014**, *78*, 340–374.
- (52) (a) Gerry, C. J.; Schreiber, S. L. Recent achievements and current trajectories of diversity-oriented synthesis. *Curr. Opin. Chem. Biol.* **2020**, *56*, 1–9. (b) Akella, L. B.; Marcaurelle, L. A. Application of a sparse matrix design strategy to the synthesis of DOS libraries. *ACS Comb. Sci.* **2011**, *13*, 357–364. (c) Dandapani, S.; Marcaurelle, L. A. Current strategies for diversity-oriented synthesis. *Curr. Opin. Chem. Biol.* **2010**, *14*, 362–370. (d) Schreiber, S. L. Molecular diversity by design. *Nature* **2009**, *457*, 153–154. (e) Tan, D. S. Diversity-oriented synthesis. *Chem. Biol.* **2007**, *2*, 483–518.
- (53) Gadagkar, S. R.; Call, G. B. Computational tools for fitting the Hill equation to dose-response curves. *J. Pharmacol. Toxicol. Methods* **2015**, *71*, 68–76.
- (54) (a) Wang, R.; Liu, Z.-Q. Solvent-free and catalyst-free Biginelli reaction to synthesize ferrocenoyl dihydropyrimidine and kinetic method to express radical-scavenging ability. *J. Org. Chem.* **2012**, *77*, 3952–3958. (b) Brown, L. E.; Dai, P.; Porco, J. A.; Schaus, S. E. Gold catalyzed cyclization of alkyne-tethered dihydropyrimidones. *Org. Lett.* **2011**, *13*, 4228–4231. (c) Li, N.; Chen, X.-H.; Song, J.; Luo, S.-W.; Fan, W.; Gong, L.-Z. Highly enantioselective organocatalytic Biginelli and Biginelli-like condensations: Reversal of the stereochemistry by tuning the 3,3′-disubstituents of phosphoric acids. *J. Am. Chem. Soc.* **2010**, *132*, 10953.
- (55) Canosa, A. V.; Faggiano, S.; Marchetti, M.; Armao, S.; Bettati, S.; Bruno, S.; Percudani, R.; Campanini, B.; Mozzarelli, A. Glutamine 89 is a key residue in the allosteric modulation of human serine racemase activity by ATP. *Sci. Rep.* **2018**, *8*, No. 9016.
- (56) (a) Turupcu, A.; Tirado-Rives, J.; Jorgensen, W. L. Explicit representation of cation- π interactions in force fields with $1/r^4$ nonbonded terms. *J. Chem. Theory Comput.* **2020**, *16*, 7184–7194. (b) Kumar, K.; Woo, S. M.; Siu, T.; Cortopassi, W. A.; Duarte, F.; Paton, R. S. Cation- π interactions in protein-ligand binding: Theory and data-mining reveal different roles for lysine and arginine. *Chem. Sci.* **2018**, *9*, 2655–2665.
- (57) (a) Cho, S. E.; Na, K. S.; Cho, S. J.; Kang, S. G. Low D-serine levels in schizophrenia: A systematic review and meta-analysis. *Neurosci. Lett.* **2016**, *634*, 42–51. (b) Ma, T. M.; Abazyan, S.; Abazyan, B.; Nomura, J.; Yang, C.; Seshadri, S.; Sawa, A.; Snyder, S. H.; Pletnikov, M. V. Pathogenic disruption of DISC 1-serine racemase binding elicits schizophrenia-like behavior via D-serine depletion. *Mol. Psychiatry* **2013**, *18*, 557–567.